

SEMI-ANALYTICAL CALCULATIONS OF THE SECULAR EVOLUTION OF
4-BODY SYSTEMS

A THESIS SUBMITTED TO
THE GRADUATE SCHOOL OF NATURAL AND APPLIED SCIENCES
OF
MIDDLE EAST TECHNICAL UNIVERSITY

BY

FULYA KIROĞLU

IN PARTIAL FULFILLMENT OF THE REQUIREMENTS
FOR
THE DEGREE OF MASTER OF SCIENCE
IN
PHYSICS

JULY 2019

Approval of the thesis:

**SEMI-ANALYTICAL CALCULATIONS OF THE SECULAR EVOLUTION
OF 4-BODY SYSTEMS**

submitted by **FULYA KIROĞLU** in partial fulfillment of the requirements for the degree of **Master of Science in Physics Department, Middle East Technical University** by,

Prof. Dr. Halil Kalıpçılar
Dean, Graduate School of **Natural and Applied Sciences**

Prof. Dr. Altuğ Özpineci
Head of Department, **Physics**

Assoc. Prof. Dr. Mehmet Atakan Gürkan
Supervisor, **Physics, METU**

Examining Committee Members:

Prof. Dr. Sıtkı Çağdaş İnam
Electrical and Electronics Engineering, Başkent University

Assoc. Prof. Dr. Mehmet Atakan Gürkan
Physics, METU

Assoc. Prof. Dr. Hande Toffoli
Physics, METU

Date:

I hereby declare that all information in this document has been obtained and presented in accordance with academic rules and ethical conduct. I also declare that, as required by these rules and conduct, I have fully cited and referenced all material and results that are not original to this work.

Name, Surname: Fulya Kirođlu

Signature :

ABSTRACT

SEMI-ANALYTICAL CALCULATIONS OF THE SECULAR EVOLUTION OF 4-BODY SYSTEMS

Kirođlu, Fulya

M.S., Department of Physics

Supervisor: Assoc. Prof. Dr. Mehmet Atakan Gürkan

July 2019, 77 pages

The observations of a large fraction of Sun-like stars in multiple-star systems and planet-forming circumstellar disks' existence around them have triggered a renewed interest in the dynamical evolution and stability of planetary systems in binaries. In this thesis, we study the secular evolution of quadruple ($N = 4$) systems consisting of two planets around a member of a binary star system where the Kozai-Lidov mechanism plays a role. The standard Kozai-Lidov mechanism has been studied extensively for hierarchical triple systems in the literature and has a number of applications to the systems with cylindrical symmetry, i.e., circular binary orbits. In this mechanism, the conservation of the component of the angular momentum vector of a test particle along the symmetry axis restricts its orientation in space, i.e., prograde orbits cannot become retrograde. One way to break the cylindrical symmetry and thus to avoid this restriction is to make the perturber's orbit eccentric and to go beyond the test particle approximation, which magnify the effects of high-order (octupole) terms in the disturbing function. These generalizations have been shown to cause large eccentricity excitations as well as orbit flips ($i > 90^\circ$) in 3-body systems. We investigate another

way of removing the axial symmetry by adding one more body to triple systems. The presence of a fourth body allows visits to the parts of phase space unavailable to triples. Depending on the initial setup of the system, the fourth body may create effects similar to that of the high-order terms in the disturbing function in the 3-body problem. We observe that the addition of a second planet on a highly inclined orbit removes the cylindrical symmetry of the companion star on a circular orbit. This in turn induces dramatic changes in the orbital eccentricity of the inner planet and even flips its orientation. On the other hand, the fourth body may suppress the high-order effects present in triples by causing periastron precession of the inner planet's orbit at a faster rate. The strength of the coupling of the planets' orbits determines the evolution and the stability of 4-body systems. In our work, we observe that especially weakly-coupled two-planet systems in binaries exhibit rich features. We calculate the secular interactions in these nearly Keplerian systems semi-analytically by combining two approximation methods: the Hamiltonian perturbation theory and the Gauss method.

Keywords: gravitation, celestial mechanics, planetary systems

ÖZ

4-CİSİM SİSTEMLERİNİN UZUN VADELİ DEVİNİMİN YARI ANALİTİK HESAPLAMALARI

Kırođlu, Fulya

Yüksek Lisans, Fizik Bölümü

Tez Yöneticisi: Doç. Dr. Mehmet Atakan Gürkan

Temmuz 2019 , 77 sayfa

Güneş benzeri yıldızların büyük kısmının çoklu yıldız sistemlerinde bulunması ve etraflarında gezegen oluşturan disklerin varlığı, yıldız ikililerinde yer alan gezegen sistemlerinin dinamik devinimi ve kararlılığı hakkında yenilenmiş bir ilgi başlatmıştır. Bu tezde, Kozai-Lidov mekanizmasının rol oynadığı ikili yıldız sistemlerinde bulunan ve iki gezegenden oluşan dördü sistemlerin uzun vadeli devinimlerini çalışıyoruz. Standart Kozai-Lidov mekanizması, hiyerarşik üçlü sistemler için literatürde kapsamlı bir şekilde çalışılmıştır ve bu mekanizmanın, silindirik simetrisine yani dairesel yörüngelere sahip ikili yıldız sistemleri için birçok uygulaması vardır. Bu mekanizmada, test parçacığının açısal momentum vektörünün simetri eksenine doğrultusundaki bileşeninin korunumu, yörüngesinin uzaydaki yönelimini sınırlar; parçacığın, yörüngesindeki ileriye dönük hareketi geriye dönemez. Silindirik simetrisini kaldırmanın ve bu sınırlamadan kaçınmanın bir yolu, etki eden cismin yörüngesini dışmerkezli yapmak ve test parçacığı yaklaşıklığının ötesine geçmektir. Bu genelleştirmelerin 3 cisimli sistemlerde, yüksek dışmerkezlilik ve yörünge çevrilmesine ($i > 90^\circ$) neden olduğu gösterilmiştir. Üçlü sistemlere bir cisim daha ekleyerek eksenel simetriyi kal-

dırmanın başka bir yolunu araştırıyoruz. Dördüncü bir cismin varlığı, faz uzayında üçlü sistemlerce erişilemeyen bölgelere erişilmesini sağlıyor. Sistemin ilk durumdaki düzenine bağlı olarak, dördüncü cisim, 3 cisim probleminin tedirgeme fonksiyonundaki yüksek mertebeye (oktopol) terimlerininkine benzer etkilere neden olabilir. Yüksek eğiklikte ikinci bir gezegen eklemenin, dairesel yörüngeye sahip ortak yıldızın silindirik simetrisini bozduğunu gözlemliyoruz. Bu da iç gezegenin eksenel dışmerkezliliğinde belirgin değişikliklere sebep olur ve hatta gezegenin yörüngesini ters çevirir. Öte yandan, dördüncü cisim, iç gezegenin enberi salınımının daha hızlı bir oranda gerçekleşmesine sebep olarak, üçlü sistemlerde var olan yüksek mertebeye etkilerini bastırabilir. Cisimlerin yörüngelerinin birlikte evrimleşme gücü, 4 cisimli sistemlerin devinim ve kararlılığını belirler. Bu çalışmamızda, özellikle yıldız ikililerinde yer alan ve birlikte zayıfça evrimleşen ikili gezegen sistemlerinin zengin özellikler gösterdiğini gözlemliyoruz. Bu neredeyse Kepler sistemlerindeki uzun süreli etkileşimleri, iki yaklaşıklık yöntemini, Hamiltonyen tedirgeme teorisi ve Gauss yöntemini, birleştirerek yarı analitik olarak hesaplıyoruz.

Anahtar Kelimeler: kütleçekimi, gök mekaniği, gezegen sistemleri

To my grandparents

ACKNOWLEDGMENTS

I am very grateful to my thesis advisor, Mehmet Atakan Gürkan. First and foremost, he aroused my curiosity in astrophysics and honestly guided me in this field. For my thesis, he allowed me to study the subject of my interest, which in turn prepared me to conduct a research on my own in my future academic career. Our meetings have been a valuable time shared for me to learn scientific ways to approach problems in physics. In this work, he suggested a solution with combined techniques of different methods. With this, the scope of our work has been enriched and this pictured us where our study fits in. Meantime, he has been a great mentor for life advice and I know I will be following his advice for many years in my life.

I also would like to thank my parents for my education and their constant support. Especially, my father has always been deeply interested in my research area and motivated me to proceed further in my studies. Most importantly, I can never underestimate my aunt's contributions in my life. I am profoundly thankful for her limitless support and encouragement.

TABLE OF CONTENTS

ABSTRACT	v
ÖZ	vii
ACKNOWLEDGMENTS	x
TABLE OF CONTENTS	xi
LIST OF TABLES	xiv
LIST OF FIGURES	xv
LIST OF ABBREVIATIONS	xvii
CHAPTERS	
1 INTRODUCTION	1
1.1 Historical development of the Kozai-Lidov mechanism	1
1.1.1 The test particle quadrupole approximation	2
1.1.2 Beyond the TPQ approximation	4
1.2 Scope of the thesis	7
2 FORMALISM	9
2.1 The geometry of Keplerian orbits	9
2.2 Vectorial constants of Keplerian orbits	12
2.3 Perturbed problem	12
2.3.1 Regularized perturbation equations	13

3	SECULAR DYNAMICS OF 3-BODY SYSTEMS	17
3.1	The Gauss method	17
3.1.1	Orbit averaging	19
3.1.2	Analytical averaging	22
3.1.2.1	Halphen's cone: geometrical averaging	23
3.1.2.2	Diagonalization of the quadratic forms	26
3.1.3	Numerical averaging: discrete Fourier transform	30
3.2	Hamiltonian perturbation theory in hierarchical triple systems	31
3.2.1	Multipole expansion of the non-Keplerian potential	32
3.2.2	Secular equations of motion	34
3.3	Comparisons with direct integrations	35
4	APPLICATIONS TO 4-BODY SYSTEMS	39
4.1	Physical picture	39
4.2	Dynamical classification of two-planet systems in binaries	41
4.2.1	Decoupled systems	42
4.2.2	Weakly-coupled systems	44
4.2.3	Coupled systems	46
4.3	Orbit flip in 4-body systems	48
4.3.1	Parameter space exploration	54
5	DISCUSSION AND CONCLUSION	61
APPENDICES		
A	SECULAR EQUATIONS OF MOTION	63

B	CALCULATION OF THE ELLIPTIC INTEGRALS	67
C	PYTHON CODES	71
	REFERENCES	73

LIST OF TABLES

TABLES

Table 4.1	Initial orbital parameters of the 4-body system displayed in Fig. 4.5	49
Table B.1	The Chebyshev coefficients for the expansion of the complete elliptic integral of the first kind, $K(k)$	68
Table B.2	The Chebyshev coefficients for the expansion of the complete elliptic integral of the second kind, $E(k)$	69

LIST OF FIGURES

FIGURES

Figure 1.1	Different astrophysical systems in which the K-L mechanism can play a role	3
Figure 1.2	The periodic oscillations of the eccentricity and inclination in the standard K-L mechanism	4
Figure 1.3	The libration of the argument of periapsis	5
Figure 1.4	The high-inclination and low-eccentricity regime of the orbit flip .	6
Figure 1.5	The low-inclination and high-eccentricity regime of the orbit flip .	7
Figure 2.1	An elliptical orbit in 3-D space.	11
Figure 3.1	Halphen's cone.	24
Figure 3.2	The comparison of the approximation methods with the direct integrations for a binary black hole system	37
Figure 3.3	The comparison of the approximation methods with the direct integrations in a 3-body system where the orbit flip occurs.	38
Figure 4.1	The evolution of a decoupled two-planet system initially on circular and coplanar orbits in the presence of a stellar companion	43
Figure 4.2	The evolution of a weakly-coupled two-planet system initially on circular and coplanar orbits in the presence of a stellar companion . .	45

Figure 4.3	The precession of the orbital angular momentum vectors of the planets in binaries	45
Figure 4.4	The evolution of a coupled two-planet system initially on circular and coplanar orbits in the presence of a stellar companion	47
Figure 4.5	The evolution of a weakly-coupled two-planet system initially on circular and inclined orbits in the presence of a stellar companion	50
Figure 4.6	Kozai-like coupled oscillations of e_1 and i_{12} in the 4-body system	51
Figure 4.7	Different $j_{12} = \text{constant}$ curves representing the variations of eccentricity and inclination of the inner planet	53
Figure 4.8	The evolution of the orbital parameters of the inner planet in two separate 3-body systems	54
Figure 4.9	The evolution of a decoupled two-planet system initially on circular and inclined orbits in the presence of a stellar companion	56
Figure 4.10	The evolution of a coupled two-planet system initially on circular and coplanar orbits in the presence of a stellar companion	57
Figure 4.11	The evolution of a coupled two-planet system initially on circular and inclined orbits in which the K-L cycles of the outer planet are suppressed	58
Figure 4.12	The evolution of the orbital eccentricity and inclination of the inner planet in the 3-body system where the orbit flip takes place	59
Figure 4.13	The evolution of the orbital eccentricity and inclination of the planets in the 4-body system in which the effect of the octupole terms is suppressed	59

LIST OF ABBREVIATIONS

K-L	Kozai-Lidov
EKM	Eccentric Kozai Mechanism
TPQ	Test Particle Quadrupole
TPO	Test Particle Octupole
DFT	Discrete Fourier Transform

CHAPTER 1

INTRODUCTION

1.1 Historical development of the Kozai-Lidov mechanism

The study of the long-term behavior of three gravitationally interacting point masses is a long-standing problem since Newton's time. The first classical perturbation theory was constructed by Lagrange and Laplace to study the planetary motions in the solar system. In modern times, the discoveries of extrasolar planet systems with surprising features – extremely short-period orbits, highly eccentric orbits, mean-motion and secular resonances – has opened a new field in celestial mechanics and motivated the research groups to explore their formation and evolution [1, 2, 3].

The Lagrange-Laplace theory is based on the expansion of the perturbing function in terms of small values of orbital eccentricities and inclinations, thus only applicable to nearly-circular and coplanar orbits as in the Solar system. In 1962, a new analytical approach was proposed by two astronomers, which works with all eccentricities and inclinations in the restricted three-body problem. Lidov [4] studied the effect of the Moon on the artificial satellites of the Earth, initially on circular orbits. Kozai [5] investigated the perturbations to asteroids orbiting the Sun under the influence of Jupiter. As their main conclusion, they found that there exists a critical angle $i_c = \cos^{-1} \sqrt{3/5} \sim 39^\circ$ such that if the initial orbital inclination of the asteroid relative to the orbital plane of Jupiter is between $39^\circ < i < 141^\circ$, the asteroid's orbit cannot remain circular as it precesses. The orbital eccentricity and inclination of the asteroid undergo periodic oscillations, which is known as Kozai–Lidov (K-L) cycles. Interestingly, the amplitude of these oscillations does not depend on Jupiter's mass, m_p , orbital semi-major axis, a_p , and eccentricity e_p , which measure

the strength of the perturbation, but is determined by their mutual initial inclination:

$$e_{\max} = (1 - (5/3) \cos^2 i_0)^{1/2}.$$

1.1.1 The test particle quadrupole approximation

K-L cycles were originally derived in the high hierarchy and test particle limits, that is, $a/a_p \ll 1$ and $m/m_p \ll 1$, respectively. In this limit, a 3-body system can be separated into two isolated binaries: the inner binary, consisting of the two closest bodies (M, m), and the outer binary, consisting of the outer (perturbing) body m_p and the inner binary taken as a point mass at their center of mass ($m + M$), Fig. 1.1 (a). In these systems, the perturbing potential of the outer body can be expanded in terms of the small semi-major axis ratio $\alpha = a/a_p$ [6]. The typical range of this ratio for which K-L cycles is important are $10 < \alpha^{-1} < 10^3$. While the lower limit corresponds to dynamically unstable triples, in the the upper limit, K-L cycles are suppressed by additional perturbations in the system. In particular, general relativistic and tidal effects, planet-planet interactions and stellar rotations may cause the orbital plane of the inner body to precess faster than the K-L mechanism [7].

In the simplest case, the test particle quadrupole approximation (TPQ), the outer body has a circular orbit and the expansion of the perturbing potential includes only quadrupole terms (α^2). In addition, the angular momentum of the outer binary is much greater than that of the inner one and thus the inner body has negligible effect on the orbit of outer one. Therefore, the orientation of the orbital plane of the outer binary can be assumed to be fixed and taken as the reference plane.

With these approximations, the effect of the outer body on the inner orbit can be computed analytically by averaging the quadrupole-order perturbing potential over the orbital phases, i.e. the mean anomalies,

$$\langle \mathcal{H}_{\text{int}} \rangle = \frac{1}{4\pi^2} \int_0^{2\pi} \int_0^{2\pi} \mathcal{H}_{\text{int}}(l, \omega, \Omega, L, G, H, l_p) dl dl_p. \quad (1.1)$$

This so-called secular approximation is valid when the precession time scales are much longer than the orbital periods of the bodies in the system.

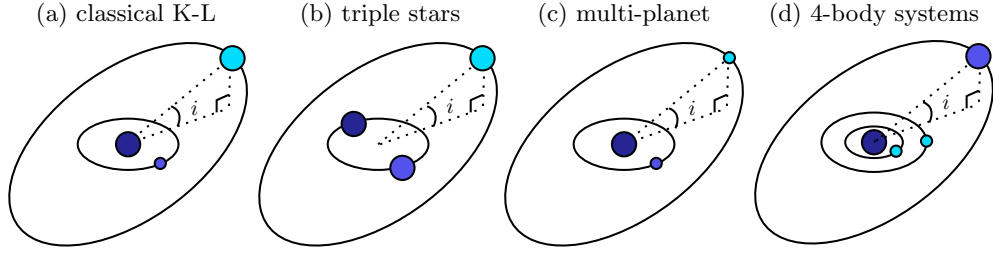


Figure 1.1: Different astrophysical systems in which the K-L mechanism can play a role. The inner and outer orbits are misaligned with respect to each other by an angle i .

The resulting double-averaged Hamiltonian in the TPQ approximation is [8]

$$\langle \mathcal{H}_{\text{int}} \rangle \simeq -\frac{\mathcal{G}m_p a^2}{8a_p^3} [2 + 3e^2 - 3(1 - e^2 + 5e^2 \sin^2 \omega) \sin^2 i]. \quad (1.2)$$

The double-averaged interaction Hamiltonian depends only on $\sin i$, e and $\sin \omega$, which are all bounded and this leads to periodic variations. Because of the secular approximation and the cylindrical symmetry of the quadrupole potential, the averaged interaction Hamiltonian is independent of the mean anomaly, l , and the longitude of the ascending node, Ω , of the inner orbit. Therefore, their conjugate momenta $L = (\mathcal{G}Ma)^{1/2}$ and $H = L(1 - e^2)^{1/2} \cos i$ are conserved. Physically, when the quadrupole potential from the outer binary is axisymmetric, there is no torque between the inclined orbits of the two binaries along the symmetry axis. Hence, the component of the inner orbit's angular momentum along the symmetry axis, which corresponds to the conjugate momentum H , is conserved. This conservation leads to the following: (i) The oscillations of eccentricity and inclination are coupled: the eccentricity of the inner binary increases while its orbital plane approaches that of the outer binary, and vice versa. (ii) The sign of H is not allowed to change: if the inner binary is initially prograde or retrograde relative to outer orbit ($i > 90^\circ$ and $i < 90^\circ$, respectively), it remains so. Switching from prograde to retrograde, i.e. orbit flip, is forbidden. In Fig. 1.2, we illustrate the coupled oscillations of the eccentricity and inclination of an inner orbit in the high inclination regime, $i_0 = 60^\circ$. The initial parameters of the system is adopted from [9]. The system is integrated over 140 Mega periods of time of the inner binary.

Since the Hamiltonian is time-independent, the energy is also conserved. Thus, the averaged problem can be described by a Hamiltonian with one degree of freedom and thus is completely integrable. If the inclination exceeds $i_c = 40^\circ$, ω may librate around either 90° or 270° [10] as in Fig. 1.3. The K-L effect gives rise to a secular 1:1 resonance in which the apsidal and nodal precession frequencies are equal and of opposite sign [11, 7]. The argument of periapsis ω corresponds to the critical angle of this resonance: $\omega \equiv \varpi - \Omega$. The orbital eccentricities and inclinations execute large amplitude oscillations at the Kozai resonance.

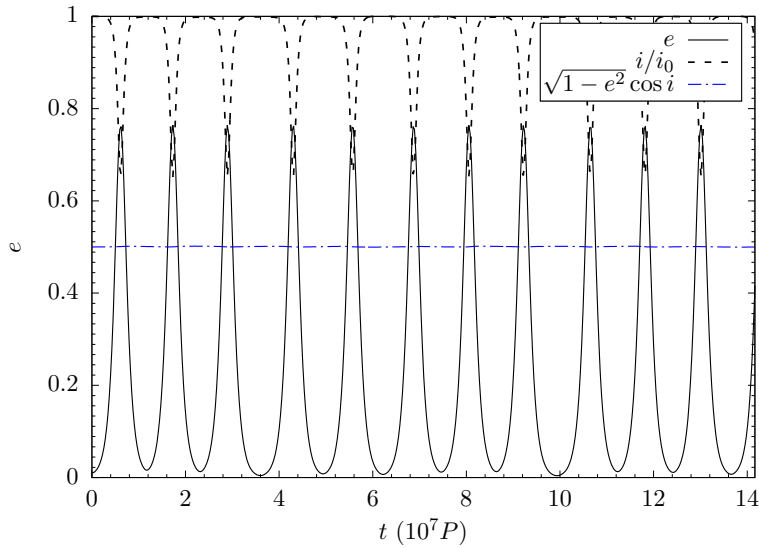


Figure 1.2: The periodic oscillations of the eccentricity and inclination (scaled by its initial value $i_0 = 60^\circ$) of an inner orbit in the 3-body system with $m/M = 10^{-3}$, $m_p/M = 0.01$, $\alpha^{-1} = 100$, $e = 10^{-5}$ and $e_p = 0.05$. The blue dashed line corresponds to the component of the angular momentum of the inner orbit along the symmetry axis of the system, which is constant.

1.1.2 Beyond the TPQ approximation

The K-L effect was later generalized to the 3-body systems with comparable masses ([6, 12]) and applied to triple stars, Fig. 1.1 (b). It was proposed to explain the production of tight stellar binaries with a period less than 7 days [13, 14]. Then, the theory was extended to systems with perturbers on eccentric orbits and applied

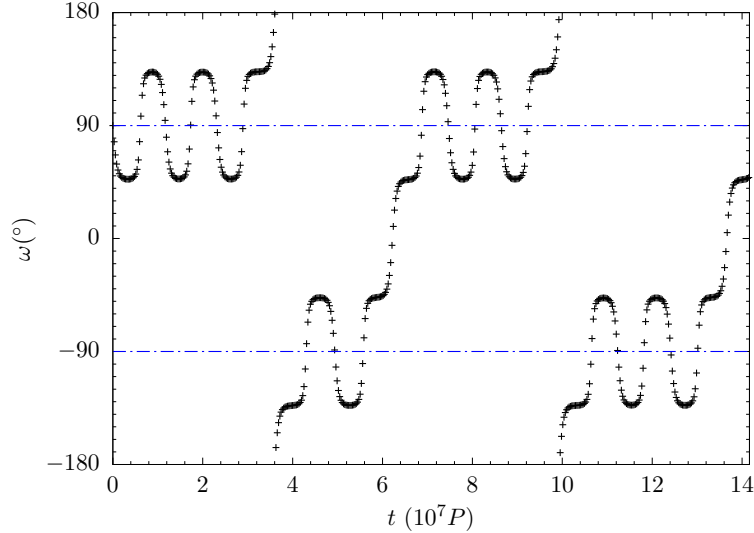


Figure 1.3: The libration of the argument of periastris of the inner orbit around 90° and 270° for the same system in Fig. 1.2.

to multi-planet systems [15], Fig. 1.1 (c). The K-L mechanism was applied to hot Jupiters in order to explain how the orbit of these giant planets within 0.1 AU of their host star are formed and why a large fraction of them are retrograde [14]. It has been suggested that large orbital eccentricity excitations of the giant planets initially on farther orbits via the K-L mechanism may bring them very close to their host stars and thus their orbit shrink by losing orbital energy. The tidal friction settles their orbits into circular ones with extremely small orbital periods and they become hot Jupiters. Moreover, Naoz *et al.* propose that the Eccentric Kozai-Lidov (EKL) mechanism may play a role in the formation of their retrograde orbits [16]. Recently [15, 17, 18], it has been shown that the TPQ approximation is insufficient to capture the secular evolution of triple systems with non-zero eccentricities and comparable masses. The octupole-order (α^3) terms in the averaged Hamiltonian give rise to a significant departure from the axial symmetry of circular orbits and the amplitude of K-L oscillations. The importance of the next order terms relative to the leading orders is measured via

$$\epsilon_{\text{oct}} = \frac{M - m}{M + m} \frac{a}{a_p} \frac{e_p}{1 - e_p^2}. \quad (1.3)$$

The small contribution of the octupole terms may dramatically change the dynamics of the system by accumulating over many K-L cycles. Particularly, when the TPQ ap-

proximation is not valid, the cylindrical symmetry present in the standard K-L mechanism disappears, and thus the axial component of the angular momentum of the inner orbit remains no longer constant. Under this relaxation of the constraints, the orbital eccentricities and the inclinations of the inner orbit can be excited to extremely large values, and even orbit flip from prograde to retrograde can be observed. In Figs. 1.4 and Fig. 1.5, we demonstrate this type of evolution of a system with two different initial set-ups, which are taken from [19]. In their work, Li *et al.* investigate the orbit flip of an inner body in the presence of an eccentric outer orbit in two different cases: the high-inclination and low-eccentricity regime Fig. 1.4 and the low-inclination and high-eccentricity regime of the inner orbit Fig. 1.5. Dynamical outcomes of these two systems differ in the amplitudes of eccentricity and inclination oscillations and the time scale of the orbit flip.

In Figs. 1.4 and 1.5, oscillations with the shorter periods are governed by the quadrupole-order terms, and the longer ones by the octupole-order terms in the averaged Hamiltonian, whose time scales are given by [20]

$$t_{\text{quad}} \sim \frac{2\pi a_p^3 (1 - a_p^2)^{3/2} \sqrt{(M + m)}}{\sqrt{\mathcal{G}} a^{3/2} m_p}, \quad (1.4)$$

$$t_{\text{oct}} \sim 2\pi \frac{4}{15} \frac{4a_p^4 (1 - e_p^2)^{5/2} \sqrt{1 - e^2} (M + m)^{3/2}}{a^{5/2} e_p \sqrt{\mathcal{G}} (M - m) m_p} \frac{1}{G/G_p + \cos i}, \quad (1.5)$$

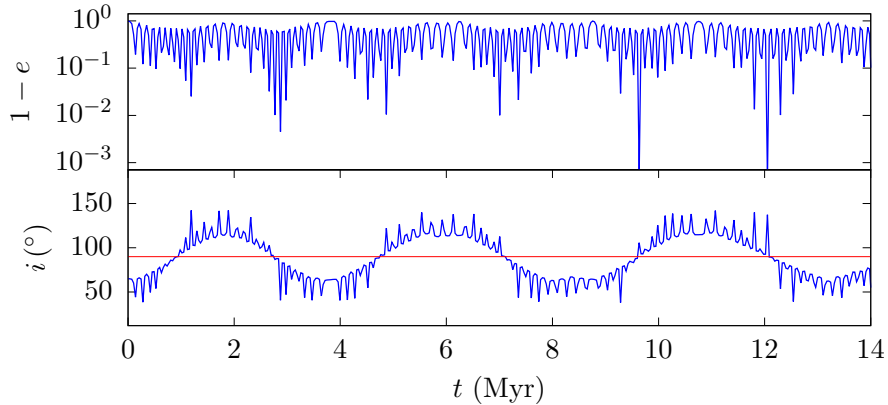


Figure 1.4: Extremely large amplitude excitations of the orbital eccentricity and inclination of an inner body by an eccentric outer orbit, $e_p = 0.6$, in the low-eccentricity, $e = 0.01$, and the high-inclination regime, $i_0 = 65^\circ$. The initial parameters of the system are taken from [19].

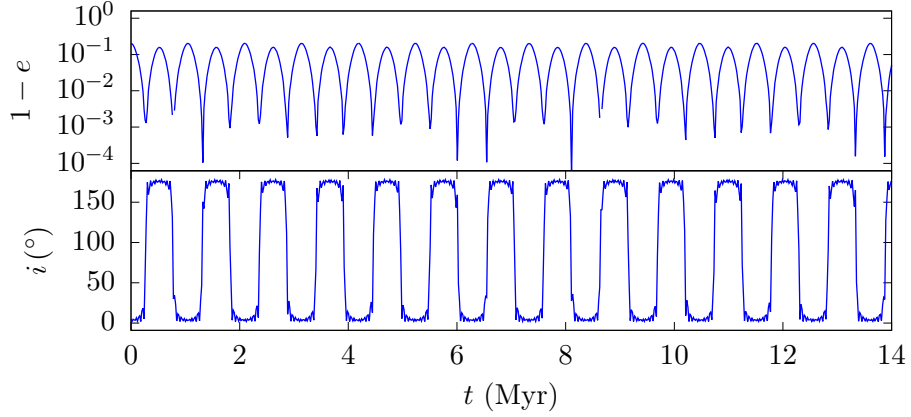


Figure 1.5: The low-inclination, $i_0 = 5^\circ$, and high-eccentricity, $e = 0.8$, case of Fig. 1.4. The orbital plane of the inner body oscillates between retrograde and prograde with a relatively small time scale and large amplitude in this case.

where G and G_p are the scalar angular momenta of the inner and outer orbits, respectively.

1.2 Scope of the thesis

Lately, the K-L mechanism has been studied in 4-body systems [2, 21, 22, 23, 24], especially for multi-planets in binary star systems Fig. 1.1 (d). Numerical simulations of these systems indicate that going beyond the 3-body problem results in richer dynamical outcomes. Motivated by this, in this thesis, we analyze the secular (long-term) evolution of 4-body systems. The outline of this thesis is as follows. In Chapter 2, we review the basic properties of Keplerian orbits and introduce the perturbed problem. Then, in Chapter 3, we present the two known perturbation methods which are used to analyze the secular dynamics of 3-body systems. We describe the Gauss method and repeat the calculations of [25] in Section 3.1., and present the Hamiltonian perturbation theory in Section 3.2. In Chapter 4, we revisit the problem of a two-planet system perturbed by a stellar companion on a wide orbit. We explore the effects of K-L mechanism in these quadrupole systems by combining the two methods in Chapter 3. At the end of Chapters 3 and 4, we test our semi-analytical approach and compare our results with the direct integrations. Finally, we discuss

our results in Chapter 5. In Appendix A, the equations of motion of a test particle in the octupole approximation are derived. Appendix B contains the calculations of the elliptical integrals. Our codes prepared for numerical simulations are presented in Appendix C.

CHAPTER 2

FORMALISM

2.1 The geometry of Keplerian orbits

Any bound particle m moving under the Newtonian gravitational force r^{-2} of a fixed point mass M follows a Keplerian orbit. We can describe the particle's Keplerian path using a set orbital elements $(a, e, f, i, \omega, \Omega)$. They correspond to the six initial conditions $(\mathbf{r}_0, \dot{\mathbf{r}}_0)$ appearing in the general solution of the Newton's equation of motion

$$\dot{\mathbf{v}} = -\mathcal{G}(M + m)r^{-3}\mathbf{r}, \quad (2.1)$$

where \mathbf{r} is the position vector pointing from M to m with $r = |\mathbf{r}|$, \mathbf{v} is the velocity vector, and \mathcal{G} is the gravitational constant. In our work, we are primarily interested in the orbital architecture of the system other than the change of the particle's position and velocity. Thus, we work with the orbital elements, which are defined as follows:

- Semi-major axis a gives half of the longest diameter of an ellipse.
- Eccentricity e describes the ellipticity of an ellipse.
- True anomaly f identifies the angular position of a particle in its elliptic path.
- Argument of periapsis ω specifies the direction of an ellipse's shortest radius (periapsis or pericenter) in the orbital plane.
- Inclination i gives the tilt of an orbit relative to a reference plane.
- Longitude of the ascending node Ω specifies where the inclined orbit intersects with the reference plane.

Transformation from the position and velocity of a particle in an elliptical orbit at a time t to these orbital elements can be found in [26].

We work with the Cartesian coordinates and take an inertial (fixed) coordinate system (X, Y, Z) . Our reference plane lies in the XY plane in which the reference direction points along the X -axis with the Y -axis taken perpendicular to it. The Z -axis is perpendicular to the XY plane forming a right-handed triad. We also define an orbital (peri-focal) coordinate system (x, y, z) . The orbital plane is chosen to lie in the xy plane where the x -axis points towards the periapsis. The z -axis is at a right angle to the orbital plane and $\hat{y} = \hat{z} \times \hat{x}$ forms a right handed triad. In this coordinate system, the unit vectors $\hat{x} = \mathbf{e}/e$ and $\hat{z} = \mathbf{j}/j$ give the directions of the (dimensionless) orbital angular momentum and the eccentricity vectors \mathbf{j} and \mathbf{e} , respectively.

We demonstrate the orbit together with its elements in Fig. 2.1. The orbital plane intersects with the reference (XY) plane along the line of nodes (blue dashed line). If the particle is moving in counterclockwise direction, we pick out the node where the particle is going up through the plane ($\dot{z} > 0$), which is called the ascending node. The first angle we need to specify the orbit is the azimuthal angle Ω which is measured from the X -axis to the ascending node. The next one is the inclination, i . It gives the angle between the Z and z axes. Orbits with $0 \leq i \leq \pi/2$ are called prograde; those with $\pi/2 \leq i \leq \pi$ are retrograde. Once we are in the orbital plane, we specify the direction of the periapsis with the argument of periapsis ω , which is angle between the ascending node and the periapsis.

The orbital elements can be obtained via

$$\begin{aligned}
e &= |\mathbf{e}|, \\
a &= \frac{j^2}{\mathcal{G}(M+m)(1-e^2)}, \\
\cos i &= \hat{\mathbf{Z}} \cdot \hat{\mathbf{z}}, \\
\cos \omega &= \hat{\mathbf{x}} \cdot \hat{\mathbf{n}}, \quad \sin \omega = \hat{\mathbf{x}} \cdot (\hat{\mathbf{z}} \times \hat{\mathbf{n}}), \\
\cos \Omega &= \hat{\mathbf{X}} \cdot \hat{\mathbf{n}}, \quad \sin \Omega = \hat{\mathbf{Y}} \cdot \hat{\mathbf{n}}
\end{aligned} \tag{2.2}$$

where the unit vector $\hat{\mathbf{n}}$ points along the line of nodes, $\hat{\mathbf{n}} = \hat{\mathbf{Z}} \times \hat{\mathbf{z}}$.

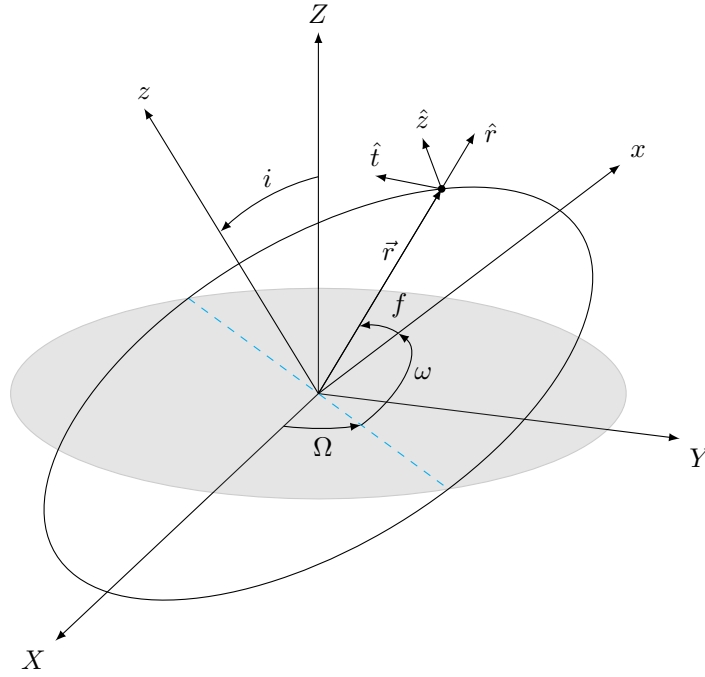


Figure 2.1: The orientation of an elliptical orbit relative to the XY reference frame (gray). The angles ω, Ω, i are measured with respect to the reference frame in the direction of motion of the particle.

In some cases, the geometry of an orbit is described using a different set of orbital elements. For example, for coplanar ($i = 0^\circ$) and circular ($e = 0$) orbits, the two angles ω and Ω are not defined. In that case, the longitude of the periapsis, $\varpi \equiv \omega + \Omega$, is used. Mean motion, $n = \sqrt{\mathcal{G}(M + m)/a^3}$, gives the angular speed of a particle required to complete one revolution in a fictitious circular orbit with constant speed (in the same orbital period P of its actual elliptical orbit). Mean anomaly, $l = n(t - \tau)$ with τ time of periapsis passage, gives the angular distance of the particle on this circular orbit from the periapsis of its elliptical orbit. Eccentric anomaly E is defined as the angle between the periapsis and the center of the ellipse (rather than the focus). The relation between the mean and the eccentric anomalies is given by Kepler's equation: $l = E - e \sin E$. In the presence of only central force, only the anomalies (f, l, E) change periodically over time, circulating through 360° , while others remain fixed.

2.2 Vectorial constants of Keplerian orbits

The orientation and the shape of a Keplerian orbit can be parametrized with the two vectorial orbital constants of the Keplerian motion: the eccentricity (the Laplace-Runge-Lenz) vector \mathbf{e} and the angular momentum vector \mathbf{j} (scaled by mna^2) given by

$$\mathbf{j} = \frac{1}{na^2} \mathbf{r} \times \mathbf{v} = \sqrt{1 - e^2} \hat{\mathbf{z}}, \quad (2.3)$$

$$\mathbf{e} = \frac{\mathbf{v} \times \mathbf{j}}{na} - \hat{\mathbf{r}} = e \hat{\mathbf{x}}. \quad (2.4)$$

Geometrically, the angular momentum vector points perpendicular to the orbit and the eccentricity vector towards from the force center to the periapsis of the orbit.

In the two-body problem, the orientation and the shape of the orbital plane remain fixed in space. Thus, we expect both the direction and the magnitude of the vectors \mathbf{j} and \mathbf{e} to be constant. In the presence of a central force, the system has a spherical symmetry. Under this rotational symmetry, the angular momentum vector is a constant of motion. As for the conservation of the eccentricity vector, the problem demands for an additional symmetry. Indeed, the Kepler problem has an extra rotational symmetry in the four-dimensional space [27]. Under this symmetry, the Keplerian orbits do not precess or change its shape: they are closed. All in all, we have four constants of motion from the Hamiltonian and the angular momentum vector. These four constants in six dimensional phase space result in planar orbits in a two-dimensional surface. Together with \mathbf{e} , we have in total seven integrals of motion. However, the angular momentum and the eccentricity vector are related via

$$j^2 + e^2 = 1, \quad \mathbf{j} \cdot \mathbf{e} = 0. \quad (2.5)$$

The remaining five independent constraints in six-dimensional phase space leave a one-dimensional one for the trajectory. This means orbits are closed.

2.3 Perturbed problem

Now we consider the perturbations of Kepler motion determined by the equation

$$\dot{\mathbf{v}} = -\frac{\mathcal{G}(M + m)\hat{\mathbf{r}}}{r^2} + \mathbf{f} \quad (2.6)$$

in the presence of an external perturbing force \mathbf{f} (per unit mass). A small deviation of the potential from $1/r$ causes precession of the orbital plane and thus the orbit does not remain closed. Specifically, the perturbed Keplerian orbit gains two additional frequencies, consisting a rotation of the line of the major axis (namely apsidal precession $\dot{\omega}$) and the line of nodes (namely nodal precession $\dot{\Omega}$) in the plane of the orbit, which are low relative to the orbital frequency (i.e., the mean motion)

As long as the external forces are sufficiently weak compared to the central force, we may model the perturbation as a small deviation from the integrable problem (Kepler orbits) and seek approximate solutions. The basic approach is to study the real orbit by finding how the undisturbed orbit changes with time. If the perturbing force suddenly vanishes at some instant t , the particle continues along its way in a Keplerian orbit with $\mathbf{r}(t)$ and $\mathbf{v}(t)$ as initial conditions. For each instant in time, an imaginary (osculating) orbit is defined by the so-called osculating elements transformed from these instantaneous set of position and velocity vectors.

In celestial mechanics, the perturbation equations are commonly obtained by the variation of the osculating elements [26]. However, these equations suffer from singularities at $e = 0$, $e = 1$ and $i = 0^\circ$. These singularities can be avoided by a canonical transformation to new Cartesian coordinates for the orbital elements. We, on the other hand, parametrize an orbit with the coordinate-free angular momentum and eccentricity vectors by following the works of [25, 28, 21, 23, 29, 17]. The resultant perturbation equations are then singularity-free, i.e. regularized.

2.3.1 Regularized perturbation equations

The time rate of changes of the vectors \mathbf{j} and \mathbf{e} under the action of an external force (per unit mass) \mathbf{f} are found by differentiating Eq. (2.3) and (2.4)

$$\begin{aligned}\frac{d(na^2\mathbf{j})}{dt} &= \mathbf{r} \times \mathbf{f}, \\ \frac{d\mathbf{e}}{dt} &= \frac{1}{\mathcal{G}(M+m)} [2\mathbf{r}(\mathbf{f} \cdot \mathbf{v}) - \mathbf{v}(\mathbf{r} \cdot \mathbf{f}) - \mathbf{f}(\mathbf{r} \cdot \mathbf{v})],\end{aligned}\tag{2.7}$$

where $\mathbf{r} = x\hat{\mathbf{x}} + y\hat{\mathbf{y}}$ is the position vector in the body coordinate system, and $\mathbf{v} = \dot{x}\hat{\mathbf{x}} + \dot{y}\hat{\mathbf{y}}$ is the velocity vector. The rate of change of the semi-major axis can be

obtained from

$$\begin{aligned}\frac{da}{dt} &= -\frac{a}{E_{\text{orb}}}\dot{E}_{\text{orb}} \\ &= \frac{2}{n^2a}\mathbf{v} \cdot \mathbf{f},\end{aligned}\quad (2.8)$$

where the orbital energy is $E_{\text{orb}} = -GMm/2a$. The components of these vectors in terms of the orbital elements are given by

$$\begin{aligned}x &= r \cos \varphi = a(\cos E - e), \\ y &= r \sin \varphi = a\sqrt{1 - e^2} \sin E, \\ \dot{x} &= -na^2 \frac{\sin E}{r}, \\ \dot{y} &= na^2 \frac{\sqrt{1 - e^2} \cos E}{r}\end{aligned}\quad (2.9)$$

where $r = a(1 - e \cos E)$.

The motion of the orbit frame (x, y, z) with respect to the reference frame (X, Y, Z) may be viewed as the rotation,

$$\frac{d\hat{\mathbf{x}}}{dt} = \boldsymbol{\eta} \times \hat{\mathbf{x}}, \quad \frac{d\hat{\mathbf{y}}}{dt} = \boldsymbol{\eta} \times \hat{\mathbf{y}}, \quad \frac{d\hat{\mathbf{z}}}{dt} = \boldsymbol{\eta} \times \hat{\mathbf{z}} \quad (2.10)$$

with the angular velocity of the orbit (x, y, z) frame

$$\boldsymbol{\eta} = \eta_x \hat{\mathbf{x}} + \eta_y \hat{\mathbf{y}} + \eta_z \hat{\mathbf{z}}. \quad (2.11)$$

Following Eggleton [30], we calculate the change in the orbital elements by using the angular momentum and the eccentricity vectors. The rates of change of these vectors are given by

$$\dot{\mathbf{e}} = \dot{e}\hat{\mathbf{x}} + e\dot{\hat{\mathbf{x}}}, \quad (2.12)$$

$$\dot{\mathbf{j}} = \dot{j}\hat{\mathbf{z}} + j\dot{\hat{\mathbf{z}}}, \quad (2.13)$$

where $\mathbf{j} = j\hat{\mathbf{z}}$ and $\mathbf{e} = e\hat{\mathbf{x}}$. Then, using Eq. (2.10), we can re-write them as

$$\frac{\dot{\mathbf{e}}}{e} = \frac{\dot{e}}{e}\hat{\mathbf{x}} + \eta_z \hat{\mathbf{y}} - \eta_y \hat{\mathbf{z}}, \quad (2.14)$$

$$\frac{\dot{\mathbf{j}}}{j} = \eta_y \hat{\mathbf{x}} - \eta_x \hat{\mathbf{y}} + \frac{\dot{j}}{j}\hat{\mathbf{z}}. \quad (2.15)$$

The first term in Eq. (2.14) describes the change in the eccentricity and the last two terms in the periaxis direction. The first two terms in Eq. (2.15) are responsible

for the rotation of the orbital plane and the last term for the variation of the angular momentum vector \mathbf{j} .

The coordinates of the (x, y, z) system can be expressed in terms of the (X, Y, Z) system by means of three sequential rotations with the Euler angles (ω, i, Ω) : (i) a rotation about the Z -axis through an angle ω , (ii) a rotation about the x -axis by an angle i , and (iii) a rotation about the z -axis by an angle Ω . The unit vectors $(\hat{\mathbf{x}}, \hat{\mathbf{y}}, \hat{\mathbf{z}})$ can be specified using the classical orbital elements relative to the fixed frame as

$$\begin{aligned}\hat{\mathbf{x}} &= \begin{pmatrix} \cos \Omega \cos \omega - \sin \Omega \cos i \sin \omega \\ \sin \Omega \cos \omega + \cos \Omega \cos i \sin \omega \\ \sin i \sin \omega \end{pmatrix}, \quad \hat{\mathbf{y}} = \begin{pmatrix} -\cos \Omega \sin \omega - \sin \Omega \cos i \cos \omega \\ -\sin \Omega \sin \omega + \cos \Omega \cos i \cos \omega \\ \sin i \cos \omega \end{pmatrix}, \\ \hat{\mathbf{z}} &= \begin{pmatrix} \sin i \sin \Omega \\ -\sin i \cos \Omega \\ \cos i \end{pmatrix}.\end{aligned}\quad (2.16)$$

Note that $\dot{\Omega}$ is directed along the Z axis, \dot{i} along the line of nodes, and $\dot{\omega}$ along the z axis. The components of these angular velocities along the body coordinate axes are

$$\begin{aligned}\dot{\Omega}_x &= \dot{\Omega} \sin i \sin \omega, & \dot{i}_x &= \dot{i} \cos \omega, & \dot{\omega}_x &= 0, \\ \dot{\Omega}_y &= \dot{\Omega} \sin i \cos \omega, & \dot{i}_y &= -\dot{i} \sin \omega, & \dot{\omega}_y &= 0, \\ \dot{\Omega}_z &= \dot{\Omega} \cos i, & \dot{i}_z &= 0, & \dot{\omega}_z &= \dot{\omega}.\end{aligned}\quad (2.17)$$

We can associate the time derivatives of these rotation angles with the components of the angular velocity, $\boldsymbol{\eta}$. Components of $\boldsymbol{\eta}$ in the directions of x, y , and z are given by

$$\begin{aligned}\eta_x &\equiv \dot{\omega}_x + \dot{i}_x + \dot{\Omega}_x = \dot{\Omega} \sin i \sin \omega + \dot{i} \cos \omega, \\ \eta_y &\equiv \dot{\omega}_y + \dot{i}_y + \dot{\Omega}_y = \dot{\Omega} \sin i \cos \omega - \dot{i} \sin \omega, \\ \eta_z &\equiv \dot{\omega}_z + \dot{i}_z + \dot{\Omega}_z = \dot{\Omega} \cos i + \dot{\omega}.\end{aligned}\quad (2.18)$$

This allows us to write

$$\begin{aligned}\dot{i} &= \eta_x \cos \omega - \eta_y \sin \omega, \\ \dot{\Omega} &= \frac{\eta_x \sin \omega + \eta_y \cos \omega}{\sin i}, \\ \dot{\omega} &= \eta_z - \dot{\Omega} \cos i.\end{aligned}\quad (2.19)$$

From Eqs. (2.14) and (2.15), we get

$$\eta_z = \frac{\dot{\mathbf{e}}}{e} \cdot \hat{\mathbf{y}}, \quad \eta_x = -\frac{\dot{\mathbf{j}}}{j} \cdot \hat{\mathbf{y}}, \quad \eta_y = \frac{\dot{\mathbf{j}}}{j} \cdot \hat{\mathbf{x}}.\quad (2.20)$$

Inserting these components into Eq. (2.19), we obtain the rates of change of orbital elements in terms of the vectors \mathbf{j} and \mathbf{e}

$$\begin{aligned}
 \dot{i} &= \frac{-\sin \omega \hat{\mathbf{x}} - \cos \omega \hat{\mathbf{y}}}{j} \cdot \dot{\mathbf{j}}, \\
 \dot{\Omega} &= \frac{\cos \omega \hat{\mathbf{x}} - \sin \omega \hat{\mathbf{y}}}{j \sin i} \cdot \dot{\mathbf{j}}, \\
 \dot{\omega} &= \frac{\dot{\mathbf{e}}}{e} \cdot \hat{\mathbf{y}} - \dot{\Omega} \cos i, \\
 \dot{e} &= \dot{\mathbf{e}} \cdot \hat{\mathbf{x}}
 \end{aligned} \tag{2.21}$$

as in [21].

CHAPTER 3

SECULAR DYNAMICS OF 3-BODY SYSTEMS

In this chapter, we present the methods we use for studying the secular (orbit-averaged) perturbations, providing the underlying assumptions and approximations. Using these methods, we obtain the secular equations of motion describing the long-term evolution of certain astrophysical systems. Then, we test their validity by comparing the numerical integrations of them to that of the exact Newtonian equations. From now on, we let unprimed variables (m, r, a, e, j, E, n) refer to the perturbing body, and the primed ones $(m', r', a', e', j', E', n')$ to the perturbed body.

3.1 The Gauss method

Gauss formulated a method of computing the secular variation of an orbit due to the influence of a third (perturbing) body [31]. He replaced the attraction of an external orbit by the attraction of a non-uniform elliptic ring whose line-density is inversely proportional to its orbital velocity. Under this approximation, the force of the elliptic ring at a point \mathbf{r}' can be found by integrating over its mass elements, $dm = m dl / 2\pi$,

$$\mathbf{f}' = \frac{\mathcal{G}m}{2\pi} \int_0^{2\pi} \frac{\mathbf{r} - \mathbf{r}'}{|\mathbf{r} - \mathbf{r}'|^3} dl, \quad (3.1)$$

where l is the mean anomaly. In his work, the analytical expression of the force of attraction of the elliptic ring was given in terms of Legendre's elliptic functions, which is computed via the arithmetic-geometric mean method. Later, Hill [32] pointed out that the exact calculation of secular evolution requires a second integration over the orbit of a perturbed body in addition to that of the perturbing one. As a result, the problem is reduced to the calculation of phase-averaged interactions between two non-uniform elliptic rings with the maximum density in the apoapsis and the min-

imum one in the periapsis. Halphen used a geometrical approach to simplify the expressions in the integrals, which we study in detail in the following sections.

Here, we present “the Gaussian ring algorithm” proposed by Touma *et al.* [25] to investigate the secular evolution of nearly Keplerian N -body systems interacting via softened gravity. They studied the interactions between stars orbiting around a central black hole. In this thesis, we employed this method in calculation of the secular perturbations in planetary systems.

The stability of planetary systems depends on the planetary separations and mass ratios. Gladman [33] showed that two-planet systems with initially circular and coplanar orbits are Hill stable, i.e., the planets do not experience a close approach if they are separated by $\delta = (a_2 - a_1)/R_{\text{Hill}} > 2\sqrt{3}$, where

$$R_{\text{Hill}} = \left(\frac{m_1 + m_2}{3M} \right)^{1/3} \frac{(a_1 + a_2)}{2}. \quad (3.2)$$

The presence of the K-L mechanism may alter the stability limit of 3-body systems. For instance, when the orbits become eccentric and inclined during K-L cycles, the stability limit becomes a complicated function of the inclination and the mass ratio [34]. As long as the system is free of mean motion resonances, the Gauss method allows us to study closely separated systems with large eccentricities and inclinations. Softening of the interaction potential avoids the instabilities due to possible encounters of the planets. This method also allows us to use an integration time step a factor of $M/(Nm)$ longer than a numerical solution of the non-averaged equations with the same accuracy. However, it is accurate to first order in the mass ratio m/M (the Keplerian orbits are well-defined) and suitable for the study of only non-resonant systems.

The procedure is then to approximate the orbit of each body as a Keplerian ring and to compute the averaged force they exert on each other using the double averaging principle, which can only be done semi-analytically. First, we calculate the gravitational potential of the perturbing ring at a point r by integrating it analytically over its mass using the Gauss method, and find the force in terms of elliptic functions. This process is called “analytical averaging”. Then, we get the secular equations of motion by performing a numerical average over the perturbed ring. Now, we introduce the orbit averaging approach in general.

3.1.1 Orbit averaging

Consider two point masses m and m' and their respective position vectors \mathbf{r} and \mathbf{r}' relative to the central body, where $r' < r$. With this notation, the equation of motion of the inner (perturbed) body is [26]

$$\ddot{\mathbf{r}}' + \mathcal{G}(M + m')\frac{\mathbf{r}'}{r'^3} = \mathcal{G}m \left[\frac{\mathbf{r} - \mathbf{r}'}{|\mathbf{r} - \mathbf{r}'|^3} - \frac{\mathbf{r}}{r^3} \right]. \quad (3.3)$$

The disturbing function which represents the gravitational potential of the perturbing body of mass m is given by

$$\Phi = -\mathcal{G}m \left[\frac{1}{|\mathbf{r}' - \mathbf{r}|} - \frac{\mathbf{r} \cdot \mathbf{r}'}{r^3} \right], \quad (3.4)$$

where $|\mathbf{r}' - \mathbf{r}| \equiv \Delta_b = \sqrt{(x - x')^2 + (y - y')^2 + (z - z')^2 + b^2}$ is the softened relative distance between m and m' , and b is the softening parameter. The leading term in the expression is called Plummer's potential. The interaction potential is softened to prevent orbit crossing. The remaining indirect term arises from the choice of the central body as the origin of the reference frame. The force per unit mass \mathbf{f}' acting on the primed body can be obtained from the gradient of this perturbing potential: $\mathbf{f}' = -\nabla\Phi$.

The unaveraged disturbing function in Eq. (3.4) contains both short and long-period terms. Therefore, while integrating the equations of motion, it requires the interval of the integration to be less than the orbital periods of the two bodies. The gravitational perturbation from a sufficiently distant perturber is small compared to the effect of the central body, hence the shape and the orientation of the perturbed orbit does not change significantly over one orbital period. This weak perturbation gradually accumulates to affect the behavior of the perturbed orbit on time-scales much longer than the orbital periods. Accordingly, we may eliminate the short-period terms by averaging the equations of motion over the orbital phases of the bodies. As the orbital elements (ω, Ω, e, i) change slowly for one revolution, they can be considered constant in the averaging process. Orbit averaging helps to diminish the accumulation of round-off errors while integrating the equations of motions for a long time and speeds up the calculations.

The averaged equations of motion in terms of non-singular vectorial variables are

$$\begin{aligned}
\left\langle \frac{da'}{dt} \right\rangle_{U'} &= \frac{1}{4\pi^2} \int_0^{2\pi} \int_0^{2\pi} \frac{da'}{dt} dl' dl, \\
\left\langle \frac{d\mathbf{j}'}{dt} \right\rangle_{U'} &= \frac{1}{4\pi^2} \int_0^{2\pi} \int_0^{2\pi} \frac{d\mathbf{j}'}{dt} dl' dl, \\
\left\langle \frac{de'}{dt} \right\rangle_{U'} &= \frac{1}{4\pi^2} \int_0^{2\pi} \int_0^{2\pi} \frac{de'}{dt} dl' dl.
\end{aligned} \tag{3.5}$$

In Eq. (3.5), $\langle \dots \rangle_{U'}$ denotes the average of a quantity over the mean anomalies of the primed and unprimed bodies. In the secular dynamics, the perturbing forces are conservative and time-independent. Hence, the system does not exchange energy in the long-term, and consequently, their semi-major axes and mean motions remain constant. The problem then reduces to understanding the remaining orbital elements e, i, ω and Ω at a given semi-major axis.

The average of any function $X(E')$ over the orbit of the perturbed body using the differential relation between the mean and eccentric anomalies, $dl = (1 - e' \cos E') dE'$, is given by

$$\langle X \rangle_{U'} = \frac{1}{2\pi} \int_0^{2\pi} X(E') (1 - e' \cos E') dE'. \tag{3.6}$$

Now, we define the radial unit vector $\hat{\mathbf{r}}'$ and the tangential vector $\hat{\mathbf{t}}' = \hat{\mathbf{z}}' \times \hat{\mathbf{r}}'$, which are given by

$$\begin{aligned}
\hat{\mathbf{r}}' &= \cos \varphi' \hat{\mathbf{x}}' + \sin \varphi' \hat{\mathbf{y}}' = \frac{(\cos E' - e') \hat{\mathbf{x}}' + \sqrt{1 - e'^2} \sin E' \hat{\mathbf{y}}'}{1 - e' \cos E'}, \\
\hat{\mathbf{t}}' &= -\sin \varphi' \hat{\mathbf{x}}' + \cos \varphi' \hat{\mathbf{y}}' = \frac{-\sqrt{1 - e'^2} \sin E' \hat{\mathbf{x}}' + (\cos E' - e') \hat{\mathbf{y}}'}{1 - e' \cos E'}.
\end{aligned} \tag{3.7}$$

The radial (R), tangential (S) and normal components (W) of the perturbing acceleration are

$$R = \hat{\mathbf{r}}' \cdot \mathbf{f}', \quad S = \hat{\mathbf{t}}' \cdot \mathbf{f}', \quad W = \hat{\mathbf{z}}' \cdot \mathbf{f}'. \tag{3.8}$$

By inserting Eqs. (3.8) and (3.7) into Eq. (3.5), we obtain the differential equations governing evolution of an osculating Keplerian orbit

$$\begin{aligned}
\frac{da'}{dt} &= \frac{2(Re' \sin E' + S\sqrt{1 - e'^2})}{n'(1 - e' \cos E')}, \\
\frac{d(n'a'^2\mathbf{j}')}{dt} &= N'_x \hat{\mathbf{x}}' + N'_y \hat{\mathbf{y}}' + N'_z \hat{\mathbf{z}}', \\
\frac{de'}{dt} &= \dot{e}'_x \hat{\mathbf{x}}' + \dot{e}'_y \hat{\mathbf{y}}' + \dot{e}'_z \hat{\mathbf{z}}'
\end{aligned} \tag{3.9}$$

with the components

$$\begin{aligned} N'_{x'} &= Wa' \sqrt{1 - e'^2} \sin E', \\ N'_{y'} &= -Wa' (\cos E' - e'), \\ N'_{z'} &= Sa' (1 - e' \cos E') \end{aligned} \quad (3.10)$$

and

$$\begin{aligned} \dot{e}'_{x'} &= \frac{\sqrt{1 - e'^2} [(4 \cos E' - e' \cos 2E' - 3e') S + 2\sqrt{1 - e'^2} \sin E' R]}{2n'a'(1 - e' \cos E')}, \\ \dot{e}'_{y'} &= \frac{[2(2 - e'^2) \sin E' - e' \sin 2E'] S - 2\sqrt{1 - e'^2} (\cos E' - e') R}{2n'a'(1 - e' \cos E')}, \\ \dot{e}'_{z'} &= -\frac{e'}{n'a'} W \sin E'. \end{aligned} \quad (3.11)$$

The averaged radial $\langle R \rangle_l$, tangential $\langle S \rangle_l$ and normal $\langle W \rangle_l$ components of the averaged force $\langle \mathbf{f}' \rangle_l$ can be represented by a Fourier series over the time interval $(0, 2\pi)$ and expanded in a time-dependent orbital parameter. The expansion in eccentric anomaly is given by

$$\langle X \rangle_l = \sum_{n=0}^{\infty} X_c^n \cos nE' + X_s^n \sin nE', \quad (3.12)$$

where $X = R, S$, and W , with the Fourier coefficients given by

$$\begin{aligned} X_c^n &= \frac{1}{2\pi} \int_0^{2\pi} \langle X \rangle_l \cos nE' dE', \\ X_s^n &= \frac{1}{2\pi} \int_0^{2\pi} \langle X \rangle_l \sin nE' dE'. \end{aligned} \quad (3.13)$$

We rewrite the average rates of change of the vectors \mathbf{j}' and \mathbf{e}' in terms of their components in the body frame as

$$\begin{aligned} n'a'^2 \left\langle \frac{d\mathbf{j}'}{dt} \right\rangle_W &= \langle N'_{x'} \rangle_W \hat{\mathbf{x}}' + \langle N'_{y'} \rangle_W \hat{\mathbf{y}}' + \langle N'_{z'} \rangle_W \hat{\mathbf{z}}', \\ \left\langle \frac{d\mathbf{e}'}{dt} \right\rangle_W &= \langle \dot{e}'_{x'} \rangle_W \hat{\mathbf{x}}' + \langle \dot{e}'_{y'} \rangle_W \hat{\mathbf{y}}' + \langle \dot{e}'_{z'} \rangle_W \hat{\mathbf{z}}'. \end{aligned} \quad (3.14)$$

From the orthogonality conditions of sine and cosine functions, the components of $\left\langle \frac{d\mathbf{j}'}{dt} \right\rangle_W$ and $\left\langle \frac{d\mathbf{e}'}{dt} \right\rangle_W$ contain the Fourier coefficients up to second order in the eccentric anomaly E' . Using Eqs. (3.10)-(3.12) and (3.6), we arrive at

$$\begin{aligned} \langle N'_{x'} \rangle_W &= a\sqrt{1 - e'^2} \left[W_s^1 - \frac{W_s^2}{2} \right], \\ \langle N'_{y'} \rangle_W &= -a' \left[(1 + e'^2) W_c^1 - \frac{3}{2} e' W_c^0 - \frac{1}{2} e' W_c^2 \right], \\ \langle N'_{z'} \rangle_W &= a' \left[\left(1 + \frac{1}{2} e'^2 \right) S_c^0 - 2e' S_c^1 + \frac{1}{2} e'^2 S_c^2 \right] \end{aligned} \quad (3.15)$$

and

$$\begin{aligned}
\langle \dot{e}'_{x'} \rangle_W &= \frac{\sqrt{1-e'^2}}{2n'a'} \left[(4S_c^1 - e'S_c^2 - 3e'S_c^0) + 2\sqrt{1-e'^2}R_s^1 \right], \\
\langle \dot{e}'_{y'} \rangle_W &= \frac{1}{2n'a'} \left[2(2-e'^2)S_s^1 - e'S_s^2 - 2\sqrt{1-e'^2}(R_c^1 - e'R_c^0) \right], \\
\langle \dot{e}'_{z'} \rangle_W &= -\frac{e'}{n'a'} \left(W_s^1 - \frac{1}{2}W_s^2 \right).
\end{aligned} \tag{3.16}$$

3.1.2 Analytical averaging

In this section, we show that the average of the force over l can be obtained analytically and expressed in terms of Legendre's elliptic functions. Here, we repeat the calculations of Touma *et al.* [25].

The average of the softened gravitational potential is given by

$$\langle \Phi \rangle_l(\mathbf{r}') = -\frac{\mathcal{G}m}{2\pi} \int_0^{2\pi} dE \frac{1 - e \cos E}{\Delta_b} \tag{3.17}$$

where $\Delta_b = [(x-x')^2 + (y-y')^2 + (z-z')^2 + b^2]^{1/2}$ is the softened relative distance between the two bodies. In the reference frame of the perturbing body, the position vectors are $\mathbf{r} = x\hat{\mathbf{x}} + y\hat{\mathbf{y}} = a(\cos E - e)\hat{\mathbf{x}} + a\sqrt{1-e^2}\sin E \hat{\mathbf{y}}$ and $\mathbf{r}' = x'\hat{\mathbf{x}} + y'\hat{\mathbf{y}} + z'\hat{\mathbf{z}}$. Using these, we have

$$\begin{aligned}
\Delta_b^2 &= [x' - a(\cos E - e)]^2 + [y' - a\sqrt{1-e^2}\sin E]^2 + z'^2 + b^2 \\
&= r'^2 + 2aex' + a^2 + a'e^2 - 2\cos E (a^2e + ax') - 2y'a\sqrt{1-e^2}\sin E + b^2.
\end{aligned} \tag{3.18}$$

Touma *et al.* write this expression in a compact form by introducing the parameters

$$\begin{aligned}
A_b &= r'^2 + a^2 + b^2 + 2aer' \cdot \hat{\mathbf{x}}, \\
B \cos \epsilon &= ar' \cdot \hat{\mathbf{x}} + a^2e, \\
B \sin \epsilon &= a\sqrt{1-e^2}\mathbf{r}' \cdot \hat{\mathbf{y}}, \\
C &= a^2e^2
\end{aligned} \tag{3.19}$$

where $x' = \mathbf{r}' \cdot \hat{\mathbf{x}}$ and $y' = \mathbf{r}' \cdot \hat{\mathbf{y}}$. In terms of these parameters, the mutual distance is given by

$$\Delta_b^2 = A_b - 2B \cos(E - \epsilon) + C \cos^2 E. \tag{3.20}$$

The average perturbing acceleration can be written as

$$\begin{aligned}
\langle \mathbf{f}' \rangle_l &= -\nabla' \langle \Phi \rangle_l = -\frac{\mathcal{G}m}{2\pi} \int_0^{2\pi} dE \frac{1 - e \cos E}{2\Delta_b^3} \nabla' \Delta_b^2 \\
&= -\frac{\mathcal{G}m}{2\pi} \int_0^{2\pi} dE \frac{1 - e \cos E}{\Delta_b^3} \left(\mathbf{r}' + ae\hat{\mathbf{x}} - a\sqrt{1 - e^2}\hat{\mathbf{y}} \sin E - a\hat{\mathbf{x}} \cos E \right) \\
&= \frac{\mathcal{G}m}{2\pi} \int_0^{2\pi} dE \frac{1 - e \cos E}{\Delta_b^3} (\mathbf{F}_0 + \mathbf{F}_1 \sin E + \mathbf{F}_2 \cos E) \tag{3.21}
\end{aligned}$$

where

$$\mathbf{F}_0 = -\mathbf{r}' - ae\hat{\mathbf{x}}, \quad \mathbf{F}_1 = a\sqrt{1 - e^2}\hat{\mathbf{y}}, \quad \mathbf{F}_2 = a\hat{\mathbf{x}}, \tag{3.22}$$

with the differential operator in Cartesian coordinates (x, y, z) given by $\nabla' = \frac{\partial}{\partial x'}\hat{\mathbf{x}} + \frac{\partial}{\partial y'}\hat{\mathbf{y}} + \frac{\partial}{\partial z'}\hat{\mathbf{z}}$ and hence $\nabla' \Delta_b^2 = 2(\mathbf{r}' + ae\hat{\mathbf{x}} - a\sqrt{1 - e^2}\hat{\mathbf{y}} \sin E - a\hat{\mathbf{x}} \cos E)$.

We define

$$\sin E \equiv \frac{x_1}{x_0}, \quad \cos E \equiv \frac{x_2}{x_0}. \tag{3.23}$$

Using these parameters, we re-write the Eq. (3.20) as

$$-x_0^2 \Delta_b^2 = A_b x_0^2 - 2B x_0 x_1 \sin \epsilon - 2B x_0 x_2 \cos \epsilon + C x_2^2 = \mathbf{x}^T \mathbf{P} \mathbf{x}, \tag{3.24}$$

where

$$\mathbf{P} \equiv \begin{pmatrix} A_b & -B \sin \epsilon & -B \cos \epsilon \\ -B \sin \epsilon & 0 & 0 \\ -B \cos \epsilon & 0 & C \end{pmatrix}. \tag{3.25}$$

Eq. (3.24) can be re-expressed without the mixing terms by an orthogonal transformation $\mathbf{x} = \mathbf{Q}\mathbf{y}$ to new coordinates (y_0, y_1, y_2) , where \mathbf{Q} is a 3×3 matrix with elements Q_{ij} , $i, j = 0, 1, 2$. There is a geometric motivation for this transformation, which we explain in the next section.

3.1.2.1 Halphen's cone: geometrical averaging

We consider an elliptical cone with its apex at the origin of our coordinate system. Following Halphen and Hill [35, 32], we use rectangular coordinates with the perturbed body P' at the origin, and denote the position of the perturbing body P and the

central body S by $\mathbf{r} = (x, y, z)$ and $\mathbf{r}_* = (x_*, y_*, z_*)$, respectively. Note that the origin was previously set at the central body. The base of the cone is defined by the orbit of the perturber. The family of vectors $\mathbf{r}(l)$ for $0 \leq l < 2\pi$, form the lateral surface of the cone. We illustrate the setup in Fig. 3.1. As we defined earlier, $\hat{\mathbf{x}}$ is directed along the periapsis of the orbit of the perturber; $\hat{\mathbf{z}}$ is perpendicular to plane of this orbit, and $\hat{\mathbf{y}} = \hat{\mathbf{z}} \times \hat{\mathbf{x}}$. In this configuration, the positions of the central and perturbing bodies are given by $\mathbf{r}_* = x_*\hat{\mathbf{x}} + y_*\hat{\mathbf{y}} + h\hat{\mathbf{z}}$ and $\mathbf{r} = x\hat{\mathbf{x}} + y\hat{\mathbf{y}} + z\hat{\mathbf{z}}$, respectively.

The ellipse defined on the plane $z = h$ by

$$\frac{(x - x_* + ae)^2}{a^2} + \frac{(y - y_*)^2}{a^2(1 - e^2)} = 1 \quad (3.26)$$

describes the orbit of the perturber.

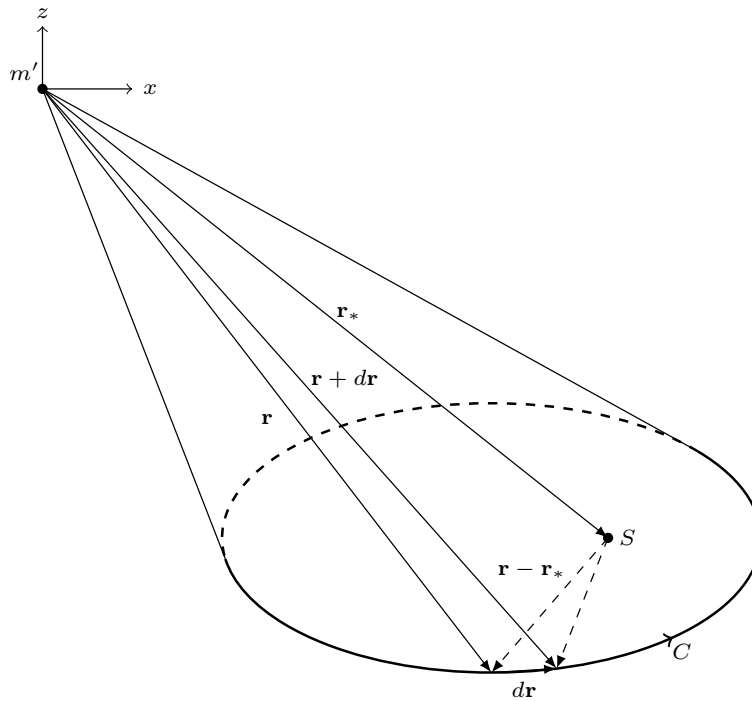


Figure 3.1: The orbit of the attracting body, which we label by the curve C , lies on the cone. The attracted body, m' , is placed at the apex of the cone, which we take as the origin.

In order to find the equation of the cone with the ellipse Eq. (3.26) as the base, consider an arbitrary ellipse lying on the cone with a perpendicular distance z from the apex and having the central body at the point (X_*, Y_*) . By using the triangle

similarity, one has $X_*/x_* = Y_*/y_* = z/h$. Then, the equation of the cone is given by

$$(1 - e^2)(xh - x_*z + aez)^2 + (yh - y_*z)^2 - (1 - e^2)a^2z^2 = 0. \quad (3.27)$$

In this configuration, the averaged direct force on m' is

$$\langle \mathbf{f}' \rangle_l = \frac{\mathcal{G}m}{2\pi} \oint_C \frac{\mathbf{r}(l) dl}{r^3}, \quad (3.28)$$

where the curve C is the orbit of the perturber, and l is the mean anomaly. By Kepler's second law, $dl/(2\pi) = d\sigma/(\pi a^2 \sqrt{1 - e^2})$, where σ is the area swept by $\mathbf{r} - \mathbf{r}_*$, and $\pi a^2 \sqrt{1 - e^2}$ is the area of the ellipse. Let $d\mathbf{r}$ denote the change in position of the attracting body in an infinitesimal time interval dt . The differential area is given by $d\sigma = \frac{1}{2}|\mathbf{w}|$, where $\mathbf{w} = (\mathbf{r} - \mathbf{r}_*) \times d\mathbf{r}$. Meantime, $h = \mathbf{w} \cdot \mathbf{r}_*/|\mathbf{w}|$ gives the perpendicular distance from the origin to the attracting ellipse. Using these, we can write $d\sigma = \frac{1}{2}\mathbf{w} \cdot \mathbf{r}_*/h$. The averaged force is then given by

$$\langle \mathbf{f}' \rangle_l = \frac{\mathcal{G}m}{2\pi h a^2 \sqrt{1 - e^2}} \oint_C \frac{\mathbf{r} \mathbf{r}_* \cdot (\mathbf{r} - \mathbf{r}_*) \times d\mathbf{r}}{r^3}. \quad (3.29)$$

Using the cyclic property of the triple product, we have

$$\mathbf{r}_* \cdot [(\mathbf{r} - \mathbf{r}_*) \times d\mathbf{r}] = d\mathbf{r} \cdot [\mathbf{r}_* \times (\mathbf{r} - \mathbf{r}_*)] = d\mathbf{r} \cdot (\mathbf{r}_* \times \mathbf{r}), \quad (3.30)$$

and hence

$$\langle \mathbf{f}' \rangle_l = \frac{\mathcal{G}m}{2\pi h a^2 \sqrt{1 - e^2}} \oint_C \frac{\mathbf{r} d\mathbf{r} \cdot (\mathbf{r}_* \times \mathbf{r})}{r^3}. \quad (3.31)$$

Now we consider the x component of the force. By employing Stokes's theorem, we arrive at

$$\langle f_x \rangle_l = \frac{\mathcal{G}m}{2\pi h a^2 \sqrt{1 - e^2}} \int_{\Sigma} ds \cdot \nabla \times \left(\frac{x \mathbf{r}_* \times \mathbf{r}}{r^3} \right) \quad (3.32)$$

where Σ is a surface on the cone bounded by C , and ds is the differential area swept out by the vector $\mathbf{r} - \mathbf{r}_*$ in one revolution of the attracting body. We choose Σ to be made up of two parts: (i) The area formed by the intersection of the cone with a particular plane to be explained later, and (ii) the lateral surface of the cone between the area in part (i) and the plane of the attracting ellipse.

We shall continue with simplifying the expression for the x component of the averaged force. In the Laplace identity,

$$\nabla \times (\mathbf{a} \times \mathbf{b}) = \mathbf{a}(\nabla \cdot \mathbf{b}) - \mathbf{b}(\nabla \cdot \mathbf{a}) + (\mathbf{b} \cdot \nabla)\mathbf{a} - (\mathbf{a} \cdot \nabla)\mathbf{b}, \quad (3.33)$$

let $\mathbf{a} = \mathbf{r}_*$ and $\mathbf{b} = x\mathbf{r}/r^3$ so that in Eq. (3.33), the second and the third terms vanish. The first term simplifies to

$$\mathbf{a}(\nabla \cdot \mathbf{b}) = \mathbf{r}_* \frac{x}{r^3}, \quad (3.34)$$

and the last term is given by

$$\begin{aligned} (\mathbf{a} \cdot \nabla)\mathbf{b} = & \hat{\mathbf{x}} \left[x_* \left(\frac{2x}{r^3} - \frac{3x^3}{r^5} \right) + y_* \left(-\frac{3x^2y}{r^5} \right) + z_* \left(-\frac{3x^2z}{r^5} \right) \right] \\ & + \hat{\mathbf{y}} \left[x_* \left(\frac{y}{r^3} - \frac{3x^2y}{r^5} \right) + y_* \left(\frac{x}{r^3} - \frac{3xy^2}{r^5} \right) + z_* \left(\frac{-3xyz}{r^5} \right) \right] \\ & + \hat{\mathbf{z}} \left[x_* \left(\frac{z}{r^3} - \frac{3x^2z}{r^5} \right) + y_* \left(-\frac{3xyz}{r^5} \right) + z_* \left(\frac{x}{r^3} - \frac{3xz^2}{r^5} \right) \right]. \end{aligned} \quad (3.35)$$

By subtracting Eq. (3.34) from Eq. (3.35) and inserting the result into Eq. (3.32), we obtain

$$\langle f_x \rangle_t = \frac{\mathcal{G}m}{2\pi h a^2 \sqrt{1-e^2}} \int_{\Sigma} d\mathbf{s} \cdot \mathbf{r} \left(\frac{3x \mathbf{r}_* \cdot \mathbf{r}}{r^5} - \frac{x_*}{r^3} \right). \quad (3.36)$$

Recall the surface Σ that we described above in two parts. There will be no contribution from the lateral surface of the cone (part (ii)) because $d\mathbf{s} \cdot \mathbf{r} = 0$ there. Thus, the averaged force of the attracting ellipse (labeled as the curve C) will be equivalent to that of any other ellipse whose surface forms part (i) of Σ . Therefore, Eq. (3.36) gives the same result for any curve that lies on the cone. Indeed, this allows us to pick a specific curve C on the cone that facilitates the calculation of the averaged force in Eq. (3.21).

3.1.2.2 Diagonalization of the quadratic forms

Now, we go back to the calculation of the averaged force in Eq. (3.21). As described above, we can choose a new plane that contains the orbit of the perturbing body to simplify the line integral in Eq. (3.21). Gauss introduced a new angular variable T , which was called the perspective anomaly by Hill. The perspective anomaly corresponds to a polar coordinate in this new plane and is defined by

$$\sin T \equiv \frac{y_1}{y_0}, \quad \cos T \equiv \frac{y_2}{y_0}. \quad (3.37)$$

From $\sin^2 E + \cos^2 E = \sin^2 T + \cos^2 T = 1$, we obtain

$$x_0^2 - x_1^2 - x_2^2 = 0, \quad y_0^2 - y_1^2 - y_2^2 = 0. \quad (3.38)$$

The former indicates that \mathbf{x} is confined to a cone, and the letter can be written as $\mathbf{x}^T \mathbf{M} \mathbf{x}$ with the requirement $\mathbf{Q}^T \mathbf{M} \mathbf{Q} = \mathbf{M}$, where $\mathbf{M} \equiv \text{diag}(1, -1, -1)$. Therefore, \mathbf{Q} is a pseudo-orthogonal matrix. Now we shall find this pseudo-orthogonal matrix \mathbf{Q} that diagonalizes the Eq. (3.24) such that

$$\mathbf{x}^T \mathbf{P} \mathbf{x} = \mathbf{y}^T \mathbf{Q}^T \mathbf{P} \mathbf{Q} \mathbf{y} \equiv \mathbf{y}^T \mathbf{D} \mathbf{y}, \quad (3.39)$$

where $\mathbf{D} \equiv \mathbf{Q}^T \mathbf{P} \mathbf{Q}$ is a diagonal matrix.

Now, we define the matrices that will be used to diagonalize the quadratic form in Eq. (3.24). First, consider a complex diagonal matrix, $\mathbf{C} \equiv \text{diag}(1, i, i)$, which satisfies $\mathbf{C}^2 = (\mathbf{C}^*)^2 = \mathbf{M}$, $\mathbf{C}^* \mathbf{C} = \mathbf{I}$, and $\mathbf{C} \mathbf{M} \mathbf{C} = \mathbf{C}^* \mathbf{M} \mathbf{C}^* = \mathbf{I}$, where \mathbf{I} denotes the unit matrix. Second, we define an orthogonal matrix, $\mathbf{L} \equiv \mathbf{C}^* \mathbf{Q} \mathbf{C}^*$, such that $\mathbf{L}^T \mathbf{L} \equiv \mathbf{C}^* \mathbf{Q}^T \mathbf{M} \mathbf{Q} \mathbf{C}^* = \mathbf{C}^* \mathbf{M} \mathbf{C}^* = \mathbf{I}$. Since \mathbf{Q} is a pseudo-orthogonal matrix, it can be written as $\mathbf{Q} = \mathbf{C} \mathbf{L} \mathbf{C}$. Inserting \mathbf{Q} into Eq. (3.39), we get $\mathbf{x}^T \mathbf{P} \mathbf{x} = \mathbf{y}^T \mathbf{C} \mathbf{L}^T \mathbf{R} \mathbf{L} \mathbf{C} \mathbf{y}$, where

$$\mathbf{R} \equiv \mathbf{C} \mathbf{P} \mathbf{C} = \begin{pmatrix} A_b & -iB \sin \epsilon & -iB \cos \epsilon \\ -iB \sin \epsilon & 0 & 0 \\ -iB \cos \epsilon & 0 & -C \end{pmatrix}. \quad (3.40)$$

From these, we get $\mathbf{L}^T \mathbf{R} \mathbf{L} = \text{diag}(\lambda_i)$, where the λ_i are the eigenvalues of \mathbf{R} , and \mathbf{L} matrix consists of the eigenvectors of \mathbf{R} in its columns. Using this expression, we finally arrive at

$$\mathbf{y}^T \mathbf{C} \mathbf{L}^T \mathbf{R} \mathbf{L} \mathbf{C} \mathbf{y} = \mathbf{y}^T \mathbf{C} \text{diag}(\lambda_i) \mathbf{C} \mathbf{y} = \mathbf{y}^T \text{diag}(\lambda_0, -\lambda_1, -\lambda_2) \mathbf{y}, \quad (3.41)$$

hence $\mathbf{D} = \text{diag}(\lambda_0, -\lambda_1, -\lambda_2)$. Finding the eigenvalues λ_i and then the eigenvectors of \mathbf{R} allows us to obtain the desired transformation matrix $\mathbf{Q} = \mathbf{C} \mathbf{L} \mathbf{C}$. The eigenvalues of \mathbf{R} are found by solving the cubic equation

$$y(\lambda) = \lambda^3 + (C - A_b)\lambda^2 + (B^2 - A_b C)\lambda + B^2 C \sin^2 \epsilon = 0, \quad (3.42)$$

which are

$$\begin{aligned} \lambda_0 &= -2\sqrt{Q} \cos\left(\frac{1}{3}\theta + \frac{2}{3}\pi\right) - \frac{1}{3}(C - A_b), \\ \lambda_1 &= -2\sqrt{Q} \cos\left(\frac{1}{3}\theta - \frac{2}{3}\pi\right) - \frac{1}{3}(C - A_b), \\ \lambda_3 &= -2\sqrt{Q} \cos\left(\frac{1}{3}\theta\right) - \frac{1}{3}(C - A_b) \end{aligned} \quad (3.43)$$

where

$$\begin{aligned}
Q &= \frac{1}{9}(C - A_b)^2 - \frac{1}{3}(B^2 - A_b C), \\
R &= \frac{1}{27}(C - A_b)^3 - \frac{1}{6}(C - A_b)(B^2 - A_b C) + \frac{1}{2}B^2 C \sin^2 \epsilon, \\
\theta &= \cos^{-1} \frac{R}{\sqrt{Q^3}}.
\end{aligned} \tag{3.44}$$

The eigenvectors of \mathbf{R} are given by

$$\boldsymbol{\beta} = \alpha_k \left(i, \frac{B \sin \epsilon}{\lambda_k}, \frac{B \cos \epsilon}{\lambda_k + C} \right), \tag{3.45}$$

where $k = 0, 1, 2$ and α_k is the normalization constant, that is $\boldsymbol{\beta}^k \cdot \boldsymbol{\beta}^k = 1$ or

$$1 = \alpha_k^2 \left[-1 + \frac{B^2 \sin^2 \epsilon}{\lambda_k^2} + \frac{B^2 \cos^2 \epsilon}{(\lambda_k + C)^2} \right]. \tag{3.46}$$

Using the relations between the eigenvalues λ_i (Eq. (38) in [25]), Eq. (3.46) can be re-expressed as

$$\alpha_k^2 = -\frac{\lambda_k(\lambda_k + C)}{(\lambda_k - \lambda_l)(\lambda_k - \lambda_m)}, \tag{3.47}$$

where $l, m = 0, 1, 2 \neq k$. The phases of the eigenvectors are chosen in [25] as $\alpha_0 = -i\sqrt{-\alpha_0^2}$, $\alpha_1 = -\sqrt{\alpha_1^2}$ and $\alpha_2 = -\sqrt{\alpha_2^2}$. The transformation matrix $\mathbf{Q} = \mathbf{CLC}$ is then obtained as

$$\mathbf{Q} = \begin{pmatrix} \sqrt{-\alpha_0^2} & \sqrt{\alpha_1^2} & \sqrt{\alpha_2^2} \\ \sqrt{-\alpha_0^2} B \sin \epsilon / \lambda_0 & \sqrt{\alpha_1^2} B \sin \epsilon / \lambda_1 & \sqrt{\alpha_2^2} B \sin \epsilon / \lambda_2 \\ \sqrt{-\alpha_0^2} B \cos \epsilon / (\lambda_0 + C) & \sqrt{\alpha_1^2} B \cos \epsilon / (\lambda_1 + C) & \sqrt{\alpha_2^2} B \cos \epsilon / (\lambda_2 + c) \end{pmatrix}. \tag{3.48}$$

Using the pseudo-orthogonality of \mathbf{Q} , that is $\mathbf{Q}^T \mathbf{M} \mathbf{Q} = \mathbf{M}$, the relation between the differential perspective and eccentric anomalies is given by [25]

$$dT = \frac{x_0}{y_0} dE. \tag{3.49}$$

Eq. (3.24) can be written as $\mathbf{x}^T \mathbf{P} \mathbf{x} = \lambda_0 y_0^2 - \lambda_1 y_1^2 - \lambda_2 y_2^2$ without the mixing terms. Using this and Eq. (3.21), orbit-averaged perturbing acceleration at position \mathbf{r} is re-

expressed as

$$\begin{aligned}
\langle \mathbf{f}' \rangle_l &= \frac{\mathcal{G}m}{2\pi} \int_0^{2\pi} dE \frac{1 - e \cos E}{\Delta_b^3} (\mathbf{F}_0 + \mathbf{F}_1 \sin E + \mathbf{F}_2 \cos E) \\
&= \frac{\mathcal{G}m}{2\pi} \int_0^{2\pi} dE \frac{x_0(x_0 - ex_2)(\mathbf{F}_0 x_0 + \mathbf{F}_1 x_1 + \mathbf{F}_2 x_2)}{(A_b x_0^2 - 2B x_0 x_1 \sin \epsilon - 2B x_0 x_2 \cos \epsilon + C x_2^2)^{3/2}} \\
&= \frac{\mathcal{G}m}{2\pi} \int_0^{2\pi} dT \frac{y_0 \sum_{j=0}^2 (Q_{0j} - eQ_{2j}) y_j \sum_{j,k=0,2} \mathbf{F}_j Q_{jk} y_k}{(\lambda_0 y_0^2 - \lambda_1 y_1^2 - \lambda_2 y_2^2)^{3/2}} \\
&= \frac{\mathcal{G}m}{2\pi} \int_0^{2\pi} dT \frac{\sum_{j=0}^2 (Q_{0j} - eQ_{2j}) y_j / y_0 \sum_{j,k=0,2} \mathbf{F}_j Q_{jk} y_k}{(\lambda_0 - \lambda_1 (y_1/y_0)^2 - \lambda_2 (y_2/y_0)^2)^{3/2}}. \tag{3.50}
\end{aligned}$$

This expression can be simplified using the definition of the perspective anomaly in Eq. (3.49) and dropping the zero terms as

$$\langle \mathbf{f}' \rangle_l = \frac{\mathcal{G}m}{2\pi} \int_0^{2\pi} dT \frac{\mathbf{F}_U + \mathbf{F}_V \sin^2 T}{[\lambda_0 - \lambda_2 - (\lambda_1 - \lambda_2) \sin^2 T]^{3/2}}, \tag{3.51}$$

where $\mathbf{F}_U = \sum_{j=0}^2 \mathbf{F}_j U_j$ and $\mathbf{F}_V = \sum_{j=0}^2 \mathbf{F}_j V_j$ with the \mathbf{F}_j given by Eq. (3.22). The terms in these summations are defined as follows:

$$\begin{aligned}
U_0 &\equiv Q_{00}^2 - eQ_{00}Q_{20} + Q_{02}^2 - eQ_{02}Q_{22}, \\
U_1 &\equiv Q_{00}Q_{10} - eQ_{10}Q_{20} + Q_{02}Q_{12} - eQ_{12}Q_{22}, \\
U_2 &\equiv Q_{00}Q_{20} - eQ_{20}^2 + Q_{02}Q_{22} - eQ_{22}^2, \\
V_0 &\equiv Q_{01}^2 - eQ_{01}Q_{21} - Q_{02}^2 + eQ_{02}Q_{22}, \\
V_1 &\equiv Q_{01}Q_{11} - eQ_{11}Q_{21} - Q_{02}Q_{12} + eQ_{12}Q_{22}, \\
V_2 &\equiv Q_{01}Q_{21} - eQ_{21}^2 - Q_{02}Q_{22} + eQ_{22}^2.
\end{aligned} \tag{3.52}$$

As a final step, the averaged force is expressed in terms of the complete elliptic integrals of the first and second kind, $E(k) = \int_0^{\pi/2} d\vartheta (1 - k^2 \sin^2 \vartheta)^{1/2}$ and $K(k) = \int_0^{\pi/2} d\vartheta (1 - k^2 \sin^2 \vartheta)^{-1/2}$. Using the relations

$$\begin{aligned}
\int_0^{\pi/2} \frac{dT}{(1 - k^2 \sin^2 T)^{3/2}} &= \frac{E(k)}{1 - k^2}, \\
\int_0^{\pi/2} \frac{\sin^2 T dt}{(1 - k^2 \sin^2 T)^{3/2}} &= \frac{E(k)}{k^2(1 - k^2)} - \frac{K(k)}{k^2},
\end{aligned}$$

the single averaged force is obtained as

$$\langle \mathbf{f}' \rangle_l = \frac{2\mathcal{G}m}{\pi} \frac{\sqrt{\lambda_0 - \lambda_2}}{(\lambda_0 - \lambda_1)(\lambda_1 - \lambda_2)} [(k^2 \mathbf{F}_U + \mathbf{F}_V)E(k) - (1 - k^2) \mathbf{F}_V K(k)], \tag{3.53}$$

where $k^2 = \frac{\lambda_1 - \lambda_2}{\lambda_0 - \lambda_2}$.

3.1.3 Numerical averaging: discrete Fourier transform

So far, we performed a single average over l and obtained the averaged force $\langle \mathbf{f}' \rangle_l$ analytically. Now, we perform the second average over l' . This time, we compute the double averaged equations in Eq. (3.14) which give the evolution of \mathbf{j}' and \mathbf{e}' . In [25], Touma *et al.* inspected that only the first three Fourier coefficients of the Fourier expansion of the single averaged force $\langle X \rangle_l$ (where $X = R, W, S$) in E' contribute to the average of these equations over l' . In this section, we will calculate these Fourier coefficients X_s^n . The integral in Eq. (3.13) can be computed only numerically. Hence, we approximate the integral by a direct summation at N equally spaced points of eccentric anomaly, E' , which is referred to as the discrete Fourier transform (DFT). In this case, we know the value of $\langle X \rangle_l$ only at a set of sample points E'_j .

The Fourier coefficients for the components of the single averaged force can be approximated using the trapezoidal rule as

$$\begin{aligned} X_s^n &= \frac{1}{2\pi} \int_0^{2\pi} \langle X(E') \rangle_l \sin nE' dE' \\ &\approx \frac{1}{2\pi} \sum_{j=0}^{N-1} \langle X(E'_j) \rangle_l \sin nE'_j \Delta E'. \end{aligned} \quad (3.54)$$

The step size is given by dividing the length of the interval, 2π , by the number of points, N : $\Delta E' = \frac{2\pi}{N}$. Moreover, we can discretize the eccentric anomaly as $E'_j = j\Delta E' = \frac{2\pi j}{N}$. Then,

$$\begin{aligned} X_s^n &= \frac{1}{2\pi} \sum_{j=0}^{N-1} \langle X(E'_j) \rangle_l \sin \left(\frac{2\pi j n}{N} \right) \frac{2\pi}{N} \\ &= \frac{1}{N} \sum_{j=0}^{N-1} \left\langle X \left(\frac{2\pi j}{N} \right) \right\rangle_l \sin \left(\frac{2\pi j n}{N} \right), \end{aligned} \quad (3.55)$$

The coefficients X_c^n are given in the same manner with $\sin nE' \rightarrow \cos nE'$. The sufficient number of points, N , for the evaluation of these Fourier coefficients can be determined by taking into account the error tolerance for the energy. In our work, we deal with broad ranges of these parameters. In fact, the number of points as large as $N = 500$ is needed for very eccentric and close rings to reach the desired accuracy.

With all these, our main purpose is to find how the perturbed orbit responds to the secular perturbation, which we calculate in the following way. The change in shape

and orientation of the perturbed orbit can be determined by the rate of change of the vectors \mathbf{j}' and \mathbf{e}' . To do this, first we find the components of the $\langle \mathbf{f}' \rangle_l$ in the radial, tangential and normal directions using Eq. (3.8). Then, we evaluate the elliptic integrals in Eq. (3.53) using the Chebyshev series expansions provided in Appendix B. Next, we insert them into Eq. (3.55) to get the Fourier coefficients $R_c^n, R_s^n, S_c^n, S_s^n, W_c^n$ and W_s^n . Using these, we obtain the components of the vectors $\dot{\mathbf{j}}'$ and $\dot{\mathbf{e}}'$ in Eqs. (3.10) and (3.11). Finally, we insert $\dot{\mathbf{j}}'$ and $\dot{\mathbf{e}}'$ in Eq. (3.14) into Eq. (2.21) to obtain the rate of change of orbital elements.

3.2 Hamiltonian perturbation theory in hierarchical triple systems

In this section, we describe the second method of computing the secular interactions in the 3-body problem. A hierarchical triple system consists of an inner binary (m' orbiting around M) and a third body m moving around the center of mass of the inner binary on a much wider orbit. In the secular approximation, hierarchical systems can be described by two separate slowly evolving Keplerian orbits. Thus, we can write the total Hamiltonian as a sum of the Hamiltonian of an integrable system describing the two decoupled motions of the inner and outer orbits, and the interaction potential representing the coupling of these orbits. One can expand the interaction potential in terms of the small ratio of semi-major axes, a'/a . The quadrupole potential contains the perturbation of the leading order in $(a'/a)^2$, and the octupole potential extends to next order in $(a'/a)^3$. The hierarchical 3-body secular dynamics has been studied extensively in the literature via the classical perturbation methods in which the Hamiltonian is formulated in terms of the orbital elements [9, 36]. In our work, we prefer to use a coordinate-free formulation of non-singular perturbation theory [29]. First, we expand the interaction potential up to octupole order and then perform orbit averaging. Then, we derive the secular equations of motion in terms of the angular momentum and the eccentricity vectors.

3.2.1 Multipole expansion of the non-Keplerian potential

We consider a test particle on a Keplerian orbit with (a', e') , and a distant mass m on a Keplerian orbit with (a, e) around the same central star, M . The origin of our coordinate system is chosen at the central star and the equator coincides with the perturber's orbit. The direct term in the gravitational potential of the perturbing body, $\Phi(\mathbf{r}', \mathbf{r}) = -\mathcal{G}m/|\mathbf{r} - \mathbf{r}'|$, can be represented by a multipole expansion up to octupole order in r'/r

$$\Phi(\mathbf{r}', \mathbf{r}) = -\frac{\mathcal{G}m}{r} \left[1 + \frac{\mathbf{r}' \cdot \mathbf{r}}{r^2} + \frac{3(\mathbf{r}' \cdot \mathbf{r})^2}{2r^4} - \frac{r'^2}{2r^2} + \left(\frac{r'}{r}\right)^3 \left(\frac{5(\mathbf{r}' \cdot \mathbf{r})^3}{2r'^3 r^3} - \frac{3(\mathbf{r}' \cdot \mathbf{r})}{2r' r} \right) \right], \quad (3.56)$$

where $|\mathbf{r}'| < |\mathbf{r}|$. We obtain the expressions of Katz *et al.* for the double-averaged potential. In the test particle approximation, the doubled averaged potential expanded up to octupole order is given by [37, 28, 17] $\langle\langle \Phi \rangle\rangle = \langle\langle \Phi_{\text{quad}} \rangle\rangle + \langle\langle \Phi_{\text{Oct}} \rangle\rangle$ with the quadrupole term

$$\langle\langle \Phi_{\text{quad}} \rangle\rangle = \frac{3}{4} \Phi_0 \left(-\frac{1}{2} j_z^2 - e'^2 + \frac{5}{2} e_z^2 + \frac{1}{6} \right) \quad (3.57)$$

and the octupole term

$$\langle\langle \Phi_{\text{Oct}} \rangle\rangle = \frac{75}{64} \Phi_0 \epsilon_{\text{Oct}} \left[e_x \left(-\frac{1}{5} + \frac{8}{5} e'^2 - 7e_z^2 + j_z^2 \right) + 2e_z j_x j_z \right] \quad (3.58)$$

where

$$\Phi_0 = \frac{\mathcal{G}m a'^2}{a^3 (1 - e^2)^{3/2}}, \quad \epsilon_{\text{Oct}} = \frac{a'}{a} \frac{e}{1 - e^2} \quad (3.59)$$

and $\mathbf{j}' = j_x \hat{\mathbf{x}} + j_y \hat{\mathbf{y}} + j_z \hat{\mathbf{z}}$ and $\mathbf{e}' = e_x \hat{\mathbf{x}} + e_y \hat{\mathbf{y}} + e_z \hat{\mathbf{z}}$. Without the test particle approximation, double averaged octupole level potential can be found in [38].

The first two terms in Eq. (3.56) are averaged to zero, and we are left with the quadrupole and octupole terms. Below, we present the derivation of averaging the quadrupole level potential, $\langle\langle \Phi_{\text{quad}} \rangle\rangle$.

Using the orbital period $P = 2\pi a^{3/2} / \sqrt{\mathcal{G}M}$ and angular momentum per unit mass

$L = r^2 \frac{d\varphi}{dt} = \sqrt{\mathcal{G}Ma(1-e^2)}$, the average of Φ over one orbit is given by

$$\begin{aligned}\langle \Phi \rangle &= \frac{1}{P} \int_0^P dt \Phi(\mathbf{r}) \\ &= \frac{\sqrt{\mathcal{G}M}}{2\pi a^{3/2}} \int_0^{2\pi} d\varphi \frac{dt}{d\varphi} \Phi(\mathbf{r}) \\ &= \frac{(1-e^2)^{3/2}}{2\pi} \int_0^{2\pi} \frac{d\varphi}{(1+e \cos \varphi)^2} \Phi(r, \varphi)\end{aligned}\quad (3.60)$$

where $r = a(1-e^2)/(1+e \cos \varphi)$.

For the perturbed orbit, we use the primed notation $\mathbf{r}' = r'(\cos \varphi' \hat{\mathbf{x}}' + \sin \varphi' \hat{\mathbf{y}}')$. The average of the potential over one orbit is given by

$$\begin{aligned}\langle \Phi_{\text{quad}} \rangle &= \frac{\mathcal{G}m}{2r^3} \left[\langle r'^2 \rangle - \frac{3(\hat{\mathbf{x}}' \cdot \mathbf{r})^2}{r^2} \langle r'^2 \cos^2 \varphi' \rangle - \frac{3(\hat{\mathbf{y}}' \cdot \mathbf{r})^2}{r^2} \langle r'^2 \sin^2 \varphi' \rangle \right. \\ &\quad \left. - \frac{6(\hat{\mathbf{x}}' \cdot \mathbf{r})(\hat{\mathbf{y}}' \cdot \mathbf{r})}{r^2} \langle r'^2 \cos \varphi' \sin \varphi' \rangle \right].\end{aligned}\quad (3.61)$$

Using the Eq. (3.60), we obtain

$$\begin{aligned}\langle r'^2 \rangle &= \frac{a'^2}{2}(2+3e'^2), \\ \langle r'^2 \cos^2 \varphi' \rangle &= \frac{a'^2}{2}(1+4e'^2) \\ \langle r'^2 \cos \varphi' \sin \varphi' \rangle &= 0, \\ \langle r'^2 \sin^2 \varphi' \rangle &= \frac{a'^2}{2}(1-e'^2).\end{aligned}\quad (3.62)$$

From the orthogonality of $(\hat{\mathbf{x}}', \hat{\mathbf{y}}', \hat{\mathbf{z}}')$, we have $(\hat{\mathbf{x}}' \cdot \mathbf{r})^2 + (\hat{\mathbf{y}}' \cdot \mathbf{r})^2 + (\hat{\mathbf{z}}' \cdot \mathbf{r})^2 = r^2$.

Using this relation, we get rid of the terms $(\hat{\mathbf{y}}' \cdot \mathbf{r})$ in Eq. (3.61) and arrive at

$$\begin{aligned}\langle \Phi_{\text{quad}} \rangle &= \frac{\mathcal{G}ma'^2}{4r^3} \left[(2+3e'^2) - \frac{3(\hat{\mathbf{x}}' \cdot \mathbf{r})^2}{r^2}(1+4e'^2) - \frac{3(1-e'^2)}{r^2} \right. \\ &\quad \left. \times [3r^2 - 3(\hat{\mathbf{x}}' \cdot \mathbf{r})^2 - 3(\hat{\mathbf{z}}' \cdot \mathbf{r})^2] \right].\end{aligned}\quad (3.63)$$

We re-write $\langle \Phi_{\text{quad}} \rangle$ in terms of the unit vectors $\hat{\mathbf{x}}' = \mathbf{e}'/e'$ and $\hat{\mathbf{z}}' = \mathbf{j}'/\sqrt{1-e'^2}$ as

$$\langle \Phi_{\text{quad}} \rangle = \frac{\mathcal{G}ma'^2}{4r^3} \left[-1 + 6e'^2 + \frac{3(\mathbf{j}' \cdot \mathbf{r}')^2}{r^2} - \frac{15(\mathbf{e}' \cdot \mathbf{r}')^2}{r^2} \right].\quad (3.64)$$

The second average over the orbit of the perturbing body gives

$$\begin{aligned}\langle\langle \Phi_{\text{quad}} \rangle\rangle &= \frac{\mathcal{G}ma'^2}{4} \left[\frac{(-1+6e'^2)}{\langle r^3 \rangle} + 3(\mathbf{j}' \cdot \hat{\mathbf{x}}')^2 \left\langle \frac{\cos^2 \varphi}{r^3} \right\rangle + 3(\mathbf{j}' \cdot \hat{\mathbf{y}}')^2 \left\langle \frac{\sin^2 \varphi}{r^3} \right\rangle \right. \\ &\quad \left. - 15(\mathbf{e}' \cdot \hat{\mathbf{x}}')^2 \left\langle \frac{\cos^2 \varphi}{r^3} \right\rangle - 15(\mathbf{e}' \cdot \hat{\mathbf{y}}')^2 \left\langle \frac{\sin^2 \varphi}{r^3} \right\rangle \right].\end{aligned}\quad (3.65)$$

From Eq. (3.60), we have

$$\begin{aligned}\left\langle \frac{\sin^2 \varphi}{r^3} \right\rangle &= \frac{1}{2a^3(1-e^2)^{3/2}}, \\ \left\langle \frac{\cos^2 \varphi}{r^3} \right\rangle &= \frac{1}{2a^3(1-e^2)^{3/2}}, \\ \left\langle \frac{1}{r^3} \right\rangle &= \frac{1}{a^3(1-e^2)^{3/2}}.\end{aligned}\tag{3.66}$$

Inserting these and $j'^2 = 1 - e'^2$ into Eq. (3.65), we get

$$\langle\langle \Phi_{\text{quad}} \rangle\rangle = \frac{3}{4}\Phi_0 \left(-\frac{1}{2}j_z^2 - e'^2 + \frac{5}{2}e_z^2 + \frac{1}{6} \right).\tag{3.67}$$

We demonstrated how to average the quadrupole-level potential over the orbit of the perturbed and perturbing bodies. The same procedure applies for the octupole level potential, which we do not present in this thesis.

3.2.2 Secular equations of motion

The evolution of the orbit is determined by a Hamiltonian $\mathcal{H} = \mathcal{H}_{\text{Kep}} + \Phi(\mathbf{r})$, where $\mathcal{H}_{\text{Kep}} = v^2/2 - \mathcal{G}M/r$ is the Kepler Hamiltonian. The time evolution of a function f under this Hamiltonian is given by

$$\frac{df}{dt} = \{f, \mathcal{H}\},\tag{3.68}$$

or more explicitly,

$$\frac{df}{dt} = \{f, \mathbf{j}\} \nabla_{\mathbf{j}} \mathcal{H} + \{f, \mathbf{e}\} \nabla_{\mathbf{e}} \mathcal{H}.\tag{3.69}$$

Given that the dimensionless vectors

$$\begin{aligned}\mathbf{j} &= \frac{1}{\sqrt{\mathcal{G}Ma}} \mathbf{r} \times \mathbf{v}, \\ \mathbf{e} &= \frac{1}{\mathcal{G}M} \mathbf{r} \times (\mathbf{r} \times \mathbf{v}) - \hat{\mathbf{r}},\end{aligned}\tag{3.70}$$

the Poisson brackets of \mathbf{j} and \mathbf{e} give

$$\{j_i, j_j\} = \frac{1}{\sqrt{\mathcal{G}Ma}} \epsilon_{ijk} j_k, \quad \{e_i, e_j\} = \frac{1}{\sqrt{\mathcal{G}Ma}} e_{ijk} j_k, \quad \{j_i, e_j\} = -\frac{1}{\sqrt{\mathcal{G}Ma}} \epsilon_{ijk} e_k.\tag{3.71}$$

For $f = j_i$ and $f = e_i$, using the relations (3.71), we get

$$\begin{aligned}\frac{d\mathbf{j}}{dt} &= -\frac{1}{\sqrt{\mathcal{G}Ma}} (\mathbf{j} \times \nabla_{\mathbf{j}}\mathcal{H} + \mathbf{e} \times \nabla_{\mathbf{e}}\mathcal{H}), \\ \frac{d\mathbf{e}}{dt} &= -\frac{1}{\sqrt{\mathcal{G}Ma}} (\mathbf{j} \times \nabla_{\mathbf{e}}\mathcal{H} + \mathbf{e} \times \nabla_{\mathbf{j}}\mathcal{H}).\end{aligned}\tag{3.72}$$

The Kepler Hamiltonian is independent of \mathbf{e} and \mathbf{j} , so we can replace $\mathcal{H} = \mathcal{H}_{\text{Kep}} + \langle\langle\Phi\rangle\rangle$ by $\langle\langle\Phi\rangle\rangle$. In Appendix A, we derive the secular equations of motion that govern the long-term evolution of the orbital parameters of the perturbed body.

3.3 Comparisons with direct integrations

We test the applicability of the two approximation methods by comparing their results with those from direct integrations of Newton's equations with the same initial conditions and arbitrary phases. In both Gauss's method and the test particle octupole approximation (TPO), ordinary differential equations for the orbital elements are integrated with the Bulirsch-Stoer (BS) algorithm [39]. The advantage of using the BS integrator is that it is often possible to choose large step sizes while maintaining reasonable accuracy. When the interactions between particles increase in strength, the step size is reduced until the desired accuracy is reached. At each step, the Richardson extrapolation provides an estimate of the accuracy of the time step used.

In the Gauss method, the desired accuracy of the calculation is controlled by two parameters: the first one is the number of points we divide the orbit of the perturbed body in the numerical averaging (the tolerance for the energy conservation), which was discussed in Section 4.1.3; the second one, ϵ_{int} , gives the error tolerance specified in the numerical integrator for the ordinary differential equations of the orbital parameters. In the direct integrations of Newton's equations of motion, we use the REBOUND package and implement the WHFast integrator [40]. WHFast is a symplectic Wisdom-Holman integrator [41] improved in speed and for energy conservation.

First, we compare our results with the original work of [25]. We consider the example they provide: a binary black hole system with a star orbiting one of the components. In this system, the orbital inclination and eccentricity of the star undergo K-L cycles.

Our simulations for this system in Fig. 3.2 using the Gaussian ring algorithm (blue points) is consistent with Fig. 1 in [25]. We perform a direct integration (solid curves) with the same initial conditions and a random mean anomaly using a time step $dt = P_1/100 \sim 90$ years. In Fig. 3.2, we also compare our results obtained by the Gauss method and the TPO approximation (namely the averaged simulations) with the direct integrations. We take the time step in the averaged simulations as $dt = 1.25 \times 10^7$ years which is $\sim 10^5$ times larger than in the direct simulations. In the Gaussian ring algorithm, while performing the numerical average we divide the orbit of the star by $N = 100$ equally spaced points of eccentric anomaly. In addition, we take the error tolerance in the BS integrator. as $\epsilon_{\text{int}} = 10^{-12}$. The three methods show good agreement in terms of the period and amplitude of the K-L oscillations.

Also, we test the Gaussian ring algorithm and the TPO approximation in a system where the EKL mechanism causes dramatic variations in the orbital elements of a perturbed body. The initial parameters of the system are adopted from [19]. In Fig. 3.3, we see that the results of the direct integration matches closely with those of the two averaged simulations over several K-L cycles in period and amplitude. However, as the time progresses, differences in the period of K-L oscillations are developed. The orbital phases are not involved in the averaged calculations. Therefore, the additional dependence on the orbital phases in the direct integrations causes these differences in period. When we carried out direct integrations with different initial orbital phases, similar period differences are observed among them with the Gauss method and the TPO approximation.

We take the time step in the averaged simulations as $dt = 5 \times 10^2$ years which is $\sim 10^4$ times larger than in the direct simulations. In the Gaussian ring algorithm, while performing the numerical average, we divide the orbit of the star by $N = 500$ equally spaced points of eccentric anomaly. Also, we soften the interaction by taking $b = 0.01a'$. In addition, we take the error tolerance in the BS integrator as $\epsilon_{\text{int}} = 10^{-12}$.

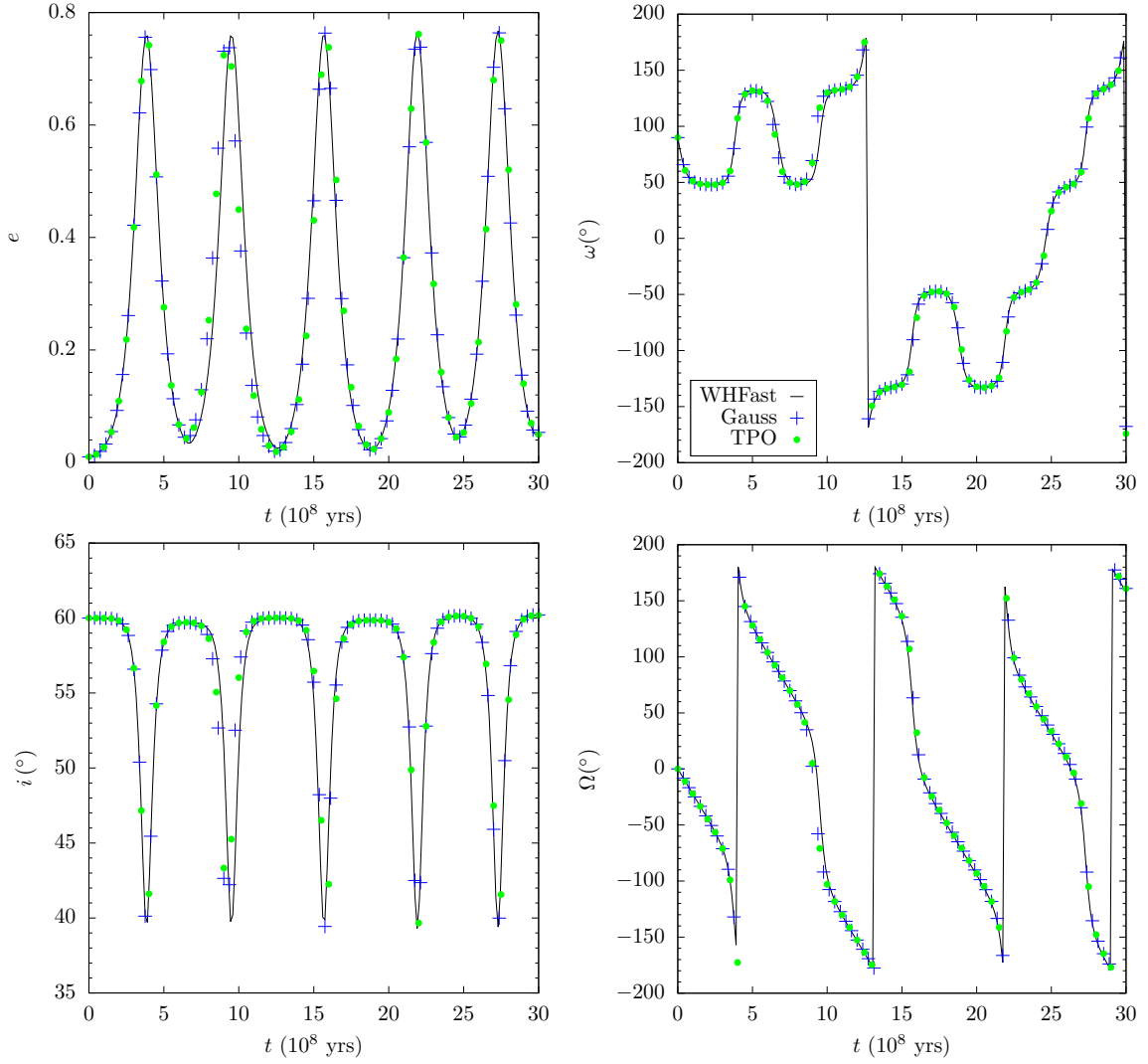


Figure 3.2: The evolution of the orbital parameters of the star in the binary black hole system using three different methods. For the primary black hole, we set $M = 1 \times 10^7 M_\odot$ and for its companion $m = 1 \times 10^7 M_\odot$, $a = 10$ pc, $e = 0.5$. The fixed orbital plane of the black hole binary is taken as the reference plane (XY). We take the initial orbital parameters of the star of mass $m' = 1M_J$ as $a' = 0.1$ pc, $e' = 0.01$, $i = 60^\circ$, $\omega = 360^\circ$ and $\Omega = 90^\circ$.

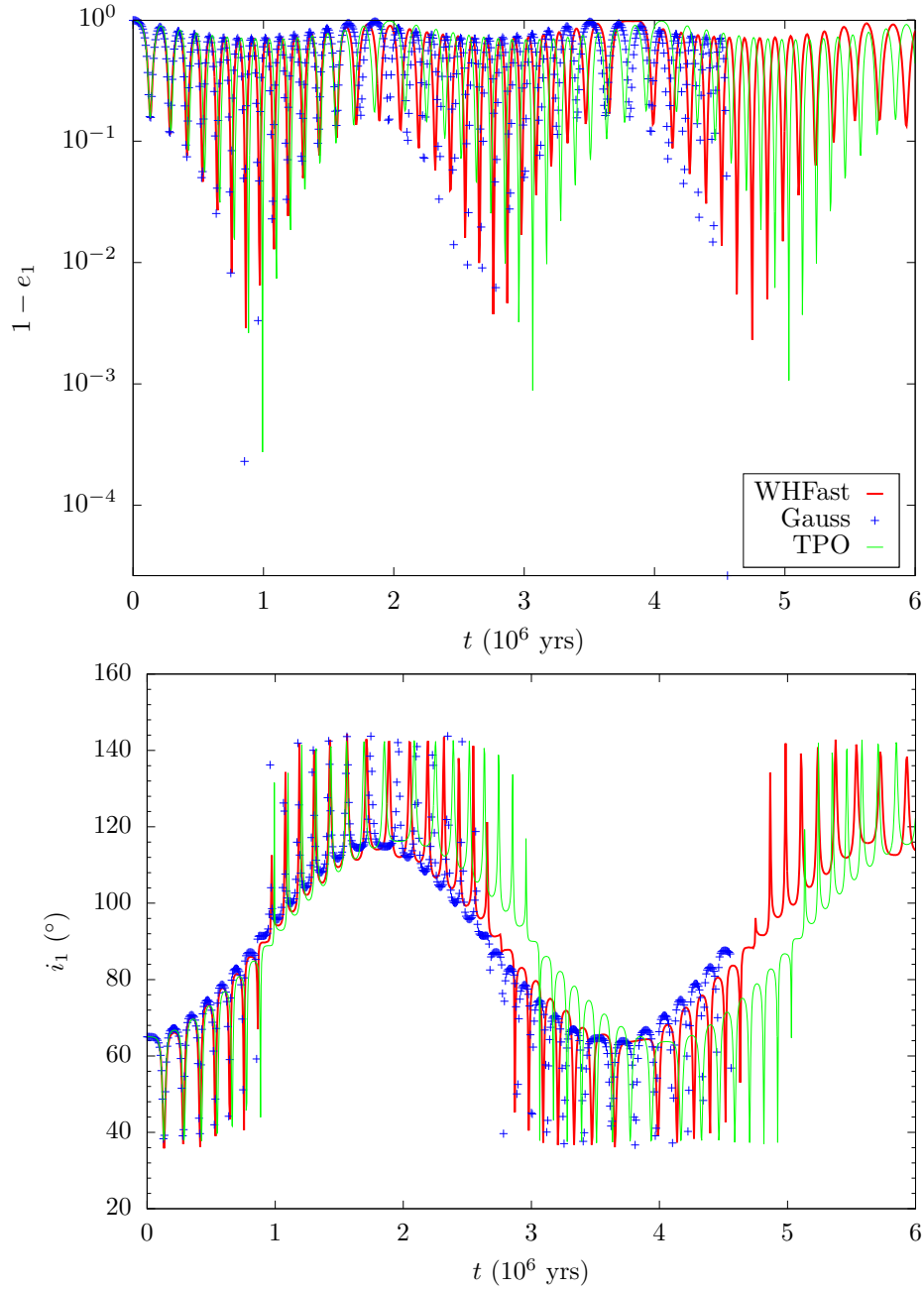


Figure 3.3: The evolution of the orbital eccentricity and inclination of the planet with $m' = 1M_j$, $a' = 4$ AU, $e' = 0.01$, $i = 65^\circ$ using three different methods. We set for the central star $M = 1M_\odot$ and for the the perturbing body $m = 1M_\odot$, $a = 50$ AU, $e = 0.6$. The fixed orbital plane of the perturbing body is taken as the reference (XY) plane. The EKL mechanism plays a role in the evolution of the star's orbit by flipping its orbit and inducing large eccentricity oscillations.

CHAPTER 4

APPLICATIONS TO 4-BODY SYSTEMS

4.1 Physical picture

In this chapter, we investigate the long-term evolution of 4-body systems consisting of a central star, two planets and a stellar companion. Throughout this chapter, we use the subscripts 0, 1, 2, and 3 to indicate the central star, the inner planet, the outer planet, and the stellar companion, respectively. When $N > 3$, the large number of dimensions of the parameter space (the mass and the three-dimensional orbit for each body) makes it difficult to study these systems. One has to implement different approximation methods (each being valid in its own regime) to describe the evolution of the system as a whole. Based on these, we divide our 4-body system into three distinct 3-body configurations:

- an isolated two-planet system orbiting around the central star: (0,1,2)
- two hierarchical 3-body systems containing a stellar companion and a single planet (m_1 or m_2) orbiting around the central star: (0,1,3) and (0,2,3)

and combine two different approximation methods that accurately account for the dynamical evolution of these separate 3-body systems. We analyze the secular evolution of a pair of planets around a single star by using the Gauss method described in Chapter 3. Instead of using the Laplace-Lagrange theory, which does not assume any hierarchy but is restricted to small values of e and i , we prefer to implement the Gauss method. On the other hand, for hierarchical triple systems (stellar binary and one planet), we used the Hamiltonian perturbation theory (TPO) discussed in Chapter 3. Analytical expressions for the equations of motion obtained by the double aver-

aged potential speed up calculations, but this method is applicable for large ratios of a_i/a_3 , where $i = 1, 2$. The more closely separated the planets from each other than from the companion star, the more accurate results the Gauss method gives in comparison to the TPO approximation for their mutual interactions. The combination of these two methods enables us to study the long-term behavior of 4-body systems semi-analytically. Recently, Pu *et al.* [23] have investigated the secular evolution of multi-planet systems with external perturbers. They implemented the linearized secular (Laplace-Lagrange) theory for the planetary interactions in the small eccentricity and small inclination regime. They then extended their analysis to the large eccentric and inclined regime only for external perturbers using the hybrid secular equations [42].

We assume that the planetary masses are much smaller than the mass of stellar companion, $m_i \ll m_3$, where $i = 1, 2$. The system's orbital angular momentum is then largely confined to the orbit of the companion star. Therefore, we assume that its orbital plane is fixed, and we take this plane to be the reference XY plane ($i_3 = 0^\circ$). The X -axis is perpendicular to the major axis; the Y -axis points towards the periastron, and the Z -axis has the same direction as the angular momentum. The angles Ω_1 and Ω_2 are measured from the reference direction (X -axis), whereas i_1 and i_2 from the Z -axis. Since $m_i \ll m_3$, while calculating the effect of the companion star on each planet, we are able to use the test particle octupole approximation. However, the mass ratios of the planets may not be small and thus we need to include the effect of the mutual planetary interactions in our calculations.

In both methods, we apply the double averaging procedure as we are only interested in secular terms. While analyzing the planetary interactions, we first perform an analytical average over the orbit of the perturbing planet (say m_2) and then a numerical average over the orbit of the perturbed planet (m_1). We repeat this averaging process to calculate the effect of the inner planet (m_1 , perturber this time) on the orbit of the outer one (m_2). To study the effect of the companion star (m_3) on each planet, we used the double averaged secular equations, Eqs. (A.8)-(A.11), which are valid up to the octupole order in semi-major axis ratios a_i/a_3 . Finally, we add up the averaged rates of change of angular momentum of the planet m_i due to the perturbing planet m_j , given by $\langle \dot{j}_i \rangle_{l_i l_j}$, and due to the stellar companion, given by $\langle \dot{j}_i \rangle_{l_i l_3}$, where

$i, j = 1, 2$ and $i \neq j$. We insert them into the averaged equations of motion in Eq. (2.21) to obtain the rates of change of orbital elements. For example, for the inner planet, we have

$$\langle \dot{i}_1 \rangle = \frac{-\sin \omega_1 \left[\langle \dot{j}_{1,x} \rangle_{l_1 l_3} + \langle \dot{j}_{1,x} \rangle_{l_1 l_2} \right] - \cos \omega_1 \left[\langle \dot{j}_{1,y} \rangle_{l_1 l_3} + \langle \dot{j}_{1,y} \rangle_{l_1 l_2} \right]}{j_1} \quad (4.1)$$

$$\langle \dot{\Omega}_1 \rangle = \frac{\cos \omega_1 \left[\langle \dot{j}_{1,x} \rangle_{l_1 l_3} + \langle \dot{j}_{1,x} \rangle_{l_1 l_2} \right] - \sin \omega_1 \left[\langle \dot{j}_{1,y} \rangle_{l_1 l_3} + \langle \dot{j}_{1,y} \rangle_{l_1 l_2} \right]}{j_1 \sin i_1} \quad (4.2)$$

$$\langle \dot{\omega}_1 \rangle = \frac{\langle \dot{e}_{1,y} \rangle_{l_1 l_2}}{e_1} + \frac{\langle \dot{e}_{1,y} \rangle_{l_1 l_3}}{e_1} - \langle \dot{\Omega}_1 \rangle \sin i_1 \quad (4.3)$$

$$\langle \dot{e}_1 \rangle = \langle \dot{e}_{1,x} \rangle_{l_1 l_2} + \langle \dot{e}_{1,x} \rangle_{l_1 l_3}, \quad (4.4)$$

where $j_{1,x}$ and $j_{1,y}$ ($e_{1,x}$ and $e_{1,y}$) respectively denote the x and y components of the angular momentum (eccentricity) vectors of the inner planet in its peri-focal (orbital) coordinate system. The expressions for the outer planet, m_2 , can be obtained by exchanging $1 \rightarrow 2$.

4.2 Dynamical classification of two-planet systems in binaries

At the moment we know about 4000 exoplanets in more than 3000 planetary systems (<http://exoplanet.eu/catalog/>). Out of these, 22% are observed to be multi-planet systems. As the number of discovered planets increases, the percentage of the multi-planet systems tends to increase, as well. In fact, it was later observed that many of the previously detected single-planet systems have an additional outer planet [43].

Even though the Sun has no stellar companion, most stars live in binary systems: about 70% of the main- and pre-main-sequence stars are in binary or multiple star systems [44]. The observation of planet-forming circumstellar discs around binary star systems [45] led many research groups to study the evolution and dynamical stability of the planets in these systems [1, 24, 2, 46, 47, 22, 48]. Specifically, we know 143 exoplanets in 97 binary-star systems, and 27% of them consist of two or more planets [49].

Newly-formed planets in circumstellar disks are expected to have small orbital eccentricities [1]. However, some extrasolar planets have extremely high eccentricities,

with the current record $e = 0.97$ [50]. Numerical simulations indicate that largest eccentricities can be excited by K-L oscillations driven by a companion star [1, 2, 3]. Indeed, the four planets with the highest known eccentricities are in binary star systems [51]. When the binary separation is larger than 30-40 AU, the orbits of the planets that are formed on the plane of the primary star's equator can have any inclination values relative to the binary plane [52]. In planet-hosting binary star systems, binary separations are observed to be larger than 50 AU. Therefore, it is possible for the orbital plane of the multiple planets to have $i > 39^\circ$ relative to the plane of the companion star. Takeda *et al.* [24] studied the effects of the K-L mechanism in two-planet systems surrounded by a component of a wide binary star system. They proposed a dynamical classification for such systems. From numerical simulations of these systems with different initial conditions, they observed three distinct classes: decoupled, weakly-coupled and coupled planets in binaries. Masses and separations of the bodies determine the strength of the coupling among them. Additionally, time scales of the perturbations from each body on one another have a factor in this classification. With this, it becomes easier to understand the stability and the evolution of 4-body systems. Below, we study each class extensively.

4.2.1 Decoupled systems

When the mass of the outer planet is much less than the inner one, $m_1/m_2 \ll 1$, and the ratio of their semi-major axes is large, $a_2/a_1 \gg 1$, they are gravitationally decoupled. In these systems, due to strong gravitational perturbation from the companion star, the mutual planetary torques cannot accumulate over time and thus have no effect on the evolution of the planets. If i_1 and i_2 are larger than the Kozai critical angle, the planets undergo independent companion star-driven K-L oscillations. As a result, the nodal lines of the planetary orbits circulate in the binary plane at different rates. At the same time, the angular momentum vector of each planet sweeps a cone around the angular momentum vector of the companion star. The relative inclination between the orbital planes of the planets is given by $\cos i_{12} = \cos i_1 \cos i_2 + \sin i_1 \sin i_2 \cos(\Omega_1 - \Omega_2)$. As the ascending nodes of the planets precess independently, the nodal offset $\Delta\Omega$ between them may grow with time. This in turn splits the planets' orbital planes and produces relative inclinations larger than the

Kozai critical angle. However, the time scale of the K-L cycles of the inner planet due to the outer one, $t_{\text{KL},12}$, is much larger than the precession time scale of its orbital plane due to the companion star, t_{13} . Therefore, the gravitational torque acting on the inner planet cannot stay coherent in a time shorter than $t_{\text{KL},12}$ and becomes suppressed. This is the reason that even if $i_{12} > 39^\circ$, the K-L oscillations between the two planets do not set in. We demonstrate this type of evolution of a 4-body system in Fig. 4.1 with the initial parameters adopted from Fig.5 in [24].

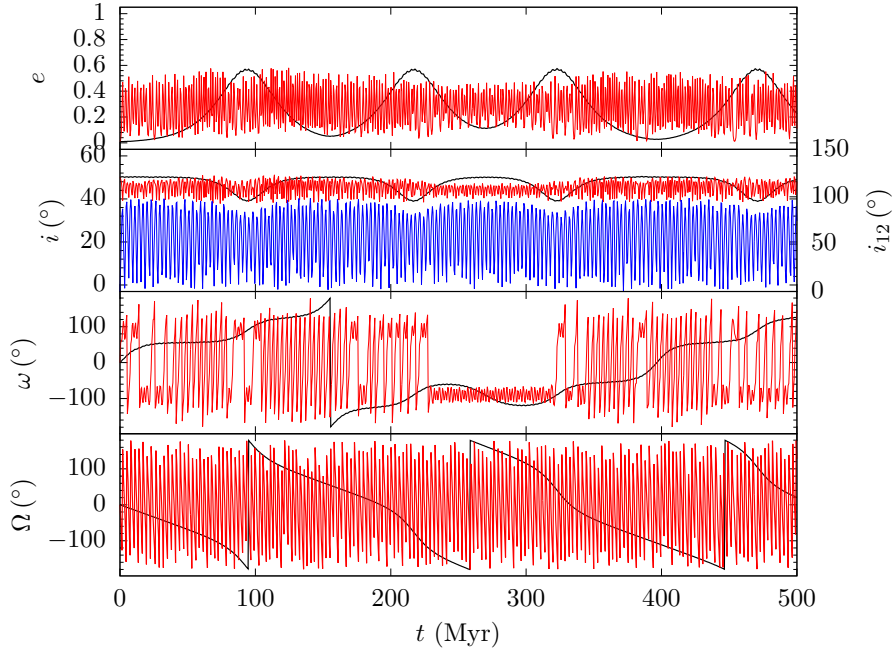


Figure 4.1: The evolution of a gravitationally decoupled two-planet system initially on circular and coplanar orbits in the presence of a stellar companion. The system initially is set with $m_1 = 1.0M_J$, $a_1 = 2.0$ AU, $e_1 = 0.01$, $i_1 = 50^\circ$ for the inner planet; $m_2 = 0.032M_J$, $a_2 = 31.6$ AU, $e_2 = 0.01$, $i_2 = 50^\circ$ for the outer planet and $m_3 = 1.0M_\odot$, $a_3 = 750$ AU, $e_3 = 0.20$, $i_3 = 0^\circ$ for the companion star. The black (red) curves correspond to the inner (outer) planet. The blue curve represents the mutual inclination i_{12} of the orbits of the planets, which oscillates between 0° and 100° .

We perform the numerical simulation using the integrator WHFast with a time step $P_1/100$ in Fig. 4.1. The first two graphs show the coupled oscillations of the orbital eccentricity and inclinations of the planets separately due to the effect of companion

star. As the time to reach the first eccentricity maximum scales as $P \sim a^{-3/2}$, the eccentricity of the outer planet (red curve) reaches its maximum while the inner planet is still almost at its initial value. In addition, the nodal precession rate $\dot{\Omega}_2$ of the outer planet's orbit is much faster than that of the inner one $\dot{\Omega}_1$. Even though the mutual inclination between the orbit of the planets i_{12} (blue lines) oscillates between 0° and 100° , additional K-L cycles between the planets are not generated and the system remains stable.

4.2.2 Weakly-coupled systems

As the ratio m_1/m_2 decreases, planets' mutual interaction may become more dominant than the outer star's perturbation. In these type of 4-body systems, while the outer planet undergoes K-L oscillations due to the companion star, the inner planet is affected by the torque from outer one. Different nodal precession rates of their initially coplanar orbits may induce a mutual inclination larger the Kozai critical angle. If the gravitational torque acting on the inner planet by the outer one is coherent, i.e., it changes in small amounts in a time shorter than the precession time scale of its orbital plane due to the companion star, it can accumulate over time and set in the K-L cycles of the inner body. We provide an example of a weakly-coupled two-planet system surrounded by a companion star in Fig. 4.2. We take the same initial set-up as in Fig.9 in [24].

At $t = 0$, orbits of the two planets are nodally aligned ($\Delta\Omega = 0^\circ$) with each other and have a small inclination $\sim 15^\circ$ with respect to the reference plane. The angles Ω_1 and Ω_2 precess initially at different rates, $\dot{\Omega}_2 > \dot{\Omega}_1$, and the mutual inclination between the orbits of the planets i_{12} start to grow. Later, the nodal precession rate $\dot{\Omega}_1$ of the inner planet's orbit increases, and the orbits of the planets become nodally aligned with each other again. The motion of \mathbf{j}_1 looks like the nutation of the spin axis of a gyroscope: the rotation around \mathbf{j}_2 and \mathbf{j}_3 due to effect of the outer planet on the inner one and the effect of the companion star on the outer planet, respectively, which is called nodal libration. We illustrate the motion of the angular momentum vectors in Fig. 4.3.

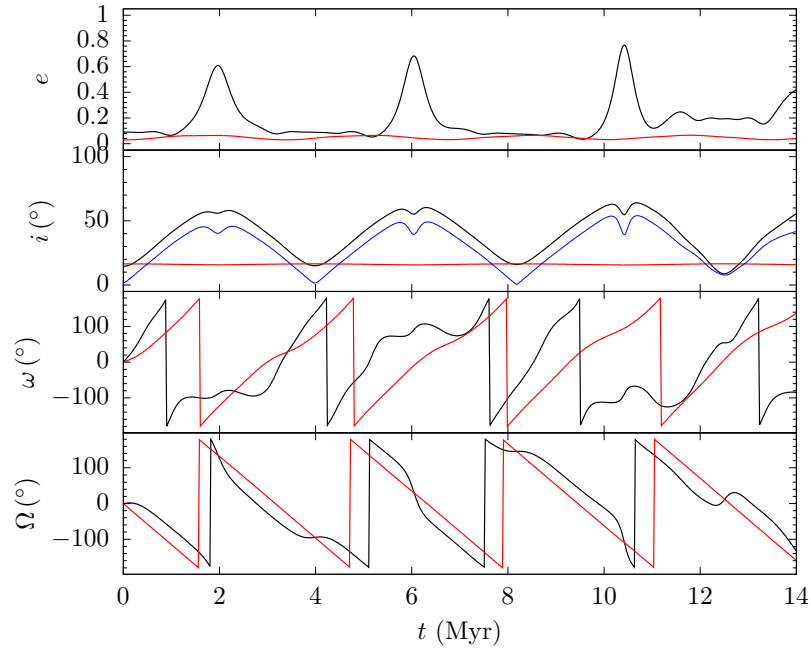


Figure 4.2: The evolution of a weakly-coupled two-planet system initially on circular and coplanar orbits in the presence of a stellar companion. The system is initially set with $m_1 = 0.02M_J$, $a_1 = 0.52$ AU, $e_1 = 0.09$, $i_1 = 14.6^\circ$ for the inner planet; $m_2 = 0.76M_J$, $a_2 = 7.53$ AU, $e_2 = 0.03$, $i_2 = 16.5^\circ$ for the outer planet and $m_3 = 0.32M_\odot$, $a_3 = 419$ AU, $e_3 = 0.81$, $i_3 = 0^\circ$ for the companion star.

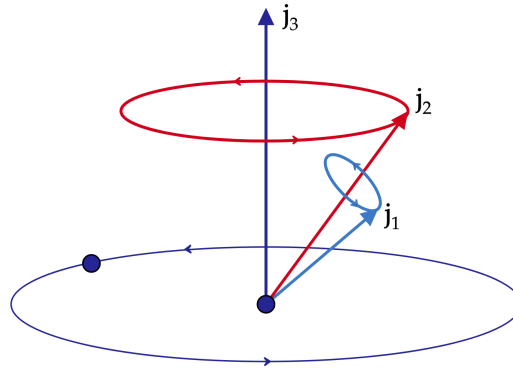


Figure 4.3: The precession of the orbital angular momentum vectors of the inner and outer planets under the effect of the outer planet and the companion star, respectively. The vectors \mathbf{j}_1 and \mathbf{j}_2 are in nodal libration.

The weak coupling of planetary systems in binaries may give rise to unfamiliar dy-

namical outcomes and even make a stable system unstable. In our example, despite the small initial inclination ($i < 39^\circ$) of the planets relative to the orbital plane of both the companion star and each other, large eccentricity excitations, $e_1 \sim 0.8$, occur. In fact, the nodal precession of the outer planet due to the companion star does not require the Kozai critical angle and results in a large nodal offset between Ω_1 and Ω_2 . In the cases where $\Delta\Omega$ is large, the mutual inclination becomes larger than 39° and thus the inner planet’s orbit undergoes large eccentricity oscillations.

4.2.3 Coupled systems

Innanen *et al.* [2] studied the stability of the planets in solar system under the effect of a hypothetical companion star with $M = 1M_\odot$, $a = 400$ AU, $e = 0.1$ and $i = 80^\circ$ and found an interesting phenomenon. The planets react in a similar way to the perturbations from the companion star. Their strong mutual interactions keep their orbits approximately coplanar: the system acts as a rigid body. The orbital planes of the planets rotate together with the same precession rate of Saturn and Jupiter. In such coupled systems, the outermost planet acts as a propagator of the perturbation from the companion star to the inner planets and increases their precession rates.

In Fig. 4.4, we provide an example of the rigid evolution of a two-planet system initially placed on coplanar orbits. We take the initial set-up in Fig.10 in [24]. Under the strong gravitational coupling of the planets’ orbits, their angular momenta precess together around \mathbf{j}_3 at the same rate. However, the precession rate of the angular momentum vector of the inner planet \mathbf{j}_1 around the outer one \mathbf{j}_2 is larger than that of \mathbf{j}_2 around \mathbf{j}_3 so that Ω_1 can follow Ω_2 . The nodal coupling of the planets is illustrated in Fig. 4.4 with a negligible small nodal offset between the longitudes of ascending nodes Ω_1 and Ω_2 . As the nodal coupling between the planets is sufficiently strong, the planetary orbits remain nearly coplanar with $5^\circ < i_{12} < 15^\circ$.

In the same figure, we also compare our results obtained by secular (averaged) interactions to the the direct N -body simulation. The solid curves correspond to the result of the direct integrations with WHFast and blue crosses indicate the results of the combination of the Gauss method and the TPO approximation.

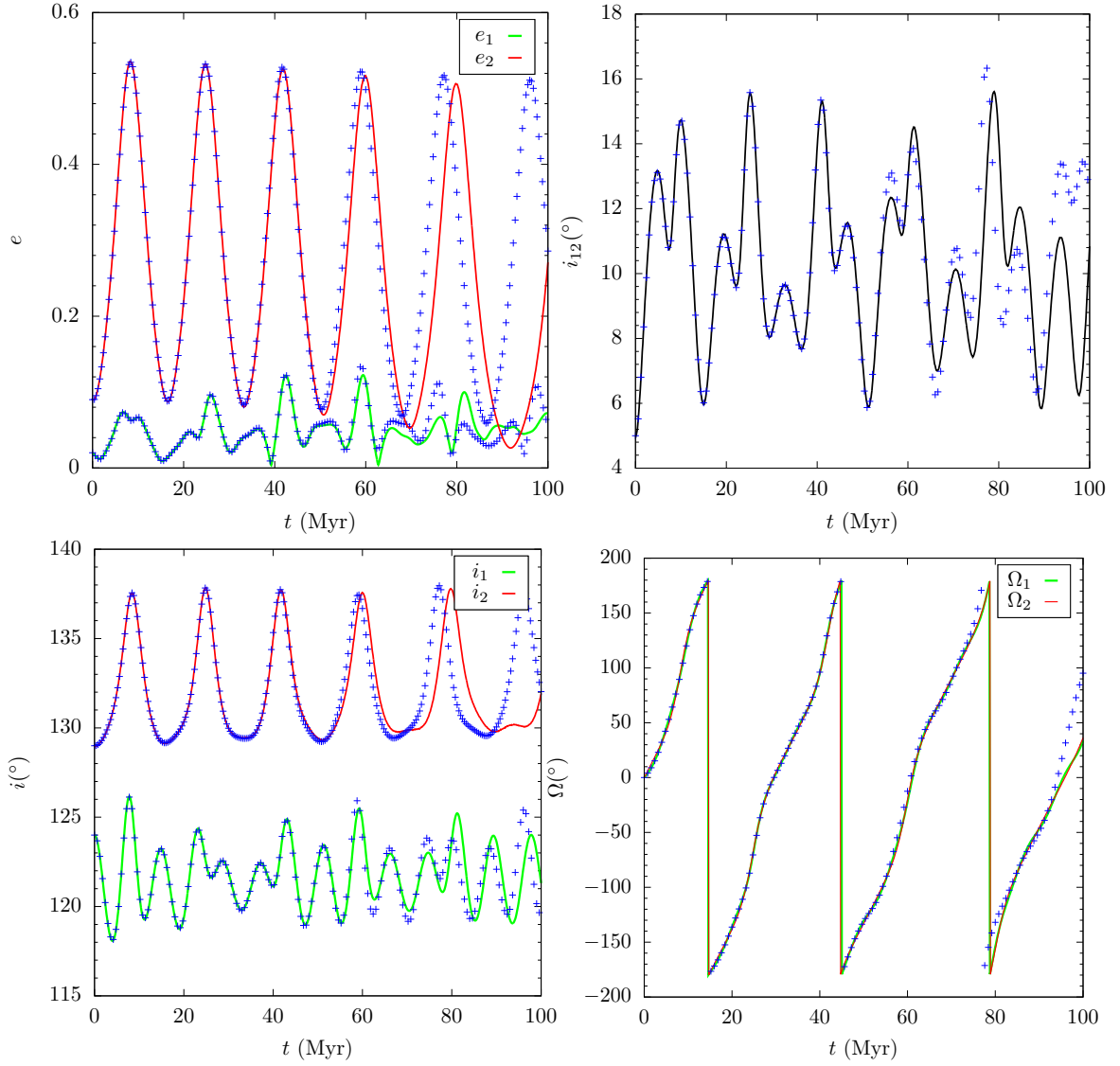


Figure 4.4: The evolution of the orbital parameters of the two planets at $a_1 = 0.7 AU$ and $a_2 = 9.1 AU$ with masses of $m_1 = 0.06M_J$ (green) and $m_2 = 0.22M_J$ (red) in the presence of a stellar companion of mass $m_3 = 0.93M_J$ at $a_3 = 950AU$. The orbital parameters are $e_1 = 0.02$, $e_2 = 0.09$, $e_3 = 0.53$, $i_1 = 124^\circ$, $i_2 = 129^\circ$. The initial orbital parameters of the system are taken from [24]. We illustrate the results of two different methods: direct integration using the WHFast integrator (red and green curves) and the combination of the Gauss method and the test particle octupole approximation (blue points).

In the combined Gauss & TPO methods, the system is evolved using a BS integrator of tolerance 10^{-10} with the time step chosen as $dt = 5 \times 10^3$ years. For the direct

integration, we take $dt = P_1/200 = 0.003$ years. The amplitude of the oscillations of e and i are in great agreement. However, as in the 3-body problem, differences in the period of the oscillations set in over time.

4.3 Orbit flip in 4-body systems

In 3-body systems with circular orbits, the averaged quadrupole potential of the perturbing body is axisymmetric. In this case, the projection of the angular momentum vector of the test particle along the symmetry axis is conserved. Because of this, the change of the sign of the axial component of the angular momentum vector is forbidden. Therefore, the mutual inclination between the orbital planes of the test particle and its perturber cannot exceed 90° over time. Provided that the EKL plays a role in the system or the test particle approximation is relaxed, the symmetry is destroyed and thus the flip of the test particle's orbit may take place.

On the other hand, we observe that the addition of a fourth body may cause a departure from the cylindrical symmetry of 3-body systems and induce dramatic changes in the eccentricities and inclinations. In this section, we look into a possibility of producing a misaligned orbit larger than 90° with respect to the binary plane in the presence of its axisymmetric potential. We observe that addition of an another planet on a highly inclined orbit may destroy the axial symmetry of the existing 3-body system. This allows to recover the flip condition in 3-body systems, which is $j_{1z} \neq \text{constant}$. Indeed, Pejcha *et al.* [48] have demonstrated with direct N -body simulations that eccentricity excitations and orbit flips can occur more in quadrupole systems than in triple ones.

First, we consider a single planet system surrounded by a wide orbit of the companion star. We set the initial parameters of system as: for the planet $m_1 = 1M_J$, $a_1 = 4 \text{ AU}$, $e_1 = 0.01$, $i_1 = 65^\circ$ and for the companion star $m_3 = 1M_\odot$, $a_3 = 950 \text{ AU}$, $e_3 = 0.01$, $i_3 = 0^\circ$. In this setup, the perturbing potential of the companion star is cylindrically symmetric and thus i_1 cannot be larger than 90° . Next, we add an another planet on a farther orbit (the outer one) m_2 to the system. We explore its parameter space of in the eccentricity, mass and inclination regions given by $0.1 < e_2 < 0.8$,

$0.1M_J < m_2 < 30M_J$ and $20^\circ < i_2 < 120^\circ$ to find the configurations in which i_1 can exceed 90° . Among the different initial setup of this 4-body system where orbit flip takes place, we provide the following example. The outer planet of mass $m_2 = 30M_J$ is placed at $a_2 = 50\text{AU}$ with $e_2 = 0.01$ and $i_2 = 120^\circ$. The orbital planes of the planets are mutually inclined by $i_{12} = 55^\circ$. We also set $\Omega_1 = \Omega_2 = 0$. The initial orbital parameters of the system are given in Table 4.1 and the result of the simulation is displayed in Fig. 4.5.

Table 4.1: Initial orbital parameters of the 4-body system displayed in Fig. 4.5

Body	m	a (AU)	e	I ($^\circ$)	ω ($^\circ$)	Ω ($^\circ$)
Central star	$1M_\odot$	–	–	–	–	–
Planet 1	$1M_J$	4	0.01	65	0	0
Planet 2	$30M_J$	50	0.01	120	0	0
Companion star	$1M_\odot$	950	0.01	0	0	0

In this setup, we make the following observations:

- The evolution of the outer planet is dominated by the perturbation from the companion star. In Fig. 4.5, we see that the standard K-L mechanism driven by the companion star plays a role in the periodic oscillations of the outer planet’s orbital eccentricity and inclination with a time scale $t_{\text{KL},23} \sim 2 \times 10^6$ years. Note that since initially $i_2 > 90^\circ$, when e_2 is at its maximum, i_2 reaches its maximum, as well. As the orbital planes of the planets are mutually inclined with respect to each other ($i_{12} > 39^\circ$), the inner planet’s eccentricity, e_1 , and mutual inclination, i_{12} , also execute outer planet-driven K-L oscillations whose time scale is short enough, $t_{\text{KL},12} \sim 5 \times 10^5$ years. In this system, we notice that the K-L time-scales for the subsystems (0,1,2) and (0,2,3) are comparable, $t_{\text{KL},12}/t_{\text{KL},23} = 0.2$, which implies that the gravitational torques in (0,1,2) and (0,2,3) are also comparable. This results in large amplitude and non-regular oscillations of e_1 and i_1 . The initially prograde orbit of the inner planet goes back and forth between retrograde and prograde in time.

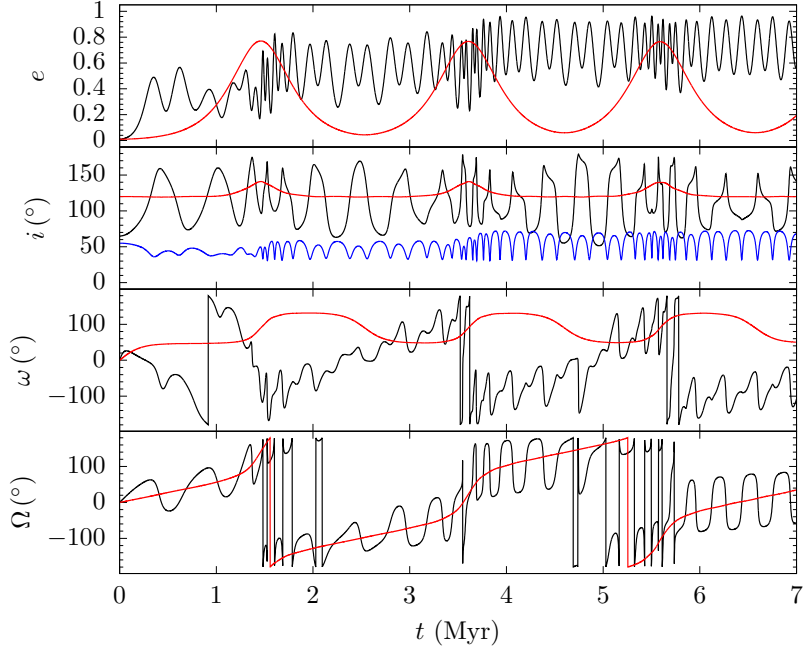


Figure 4.5: The evolution of a weakly-coupled two-planet system initially on circular and inclined orbits in the presence of a stellar companion. The initial orbital parameters of the system are given in Table 4.1. The black (red) curves correspond to the inner (outer) planet. The blue curve represents the mutual inclination of the planets. In the Gauss method, we used a softening $b = 0.01a_1$ for the planetary interactions, and in the DFT, we divided the orbit of each planet into $N_1 = 300$ and $N_2 = 200$ equally spaced points of eccentric anomaly. The system was evolved using a BS integrator with the time step $dt = 5 \times 10^3$ years.

- The two planets are weakly-coupled, and their mutual interactions play an important role in the evolution of the inner planet’s orbit. Since initially $i_{12} = 55^\circ$, the K-L oscillations of e_1 and i_{12} take place. In Fig. 4.6 (top), we see that each maximum of e_1 coincides with each minimum of i_{12} . This behavior is similar to the standard K-L cycles, aside from the differences in the amplitude of the oscillations. If we let $m_3 \rightarrow 0$, then the orbital parameters of the outer planet remain approximately fixed and thus the amplitude of the eccentricity e_1 oscillations remains constant as in the standard K-L mechanism.

This leads us to examine the component of the angular momentum vector of the inner orbit \mathbf{j}_1 along the angular momentum vector of the outer orbit \mathbf{j}_2 , which is given by $j_{12} = \sqrt{1 - e_1^2} \cos(i_{12})$. During the first 1 Myr of Fig. 4.6 (bottom),

the inclination of the outer orbit does not change significantly, so j_{12} oscillates with a small amplitude and can be assumed to be nearly constant. Therefore, the coupling of the eccentricity, e_1 , to the mutual inclination i_{12} in Fig. 4.6 (top) makes sense.

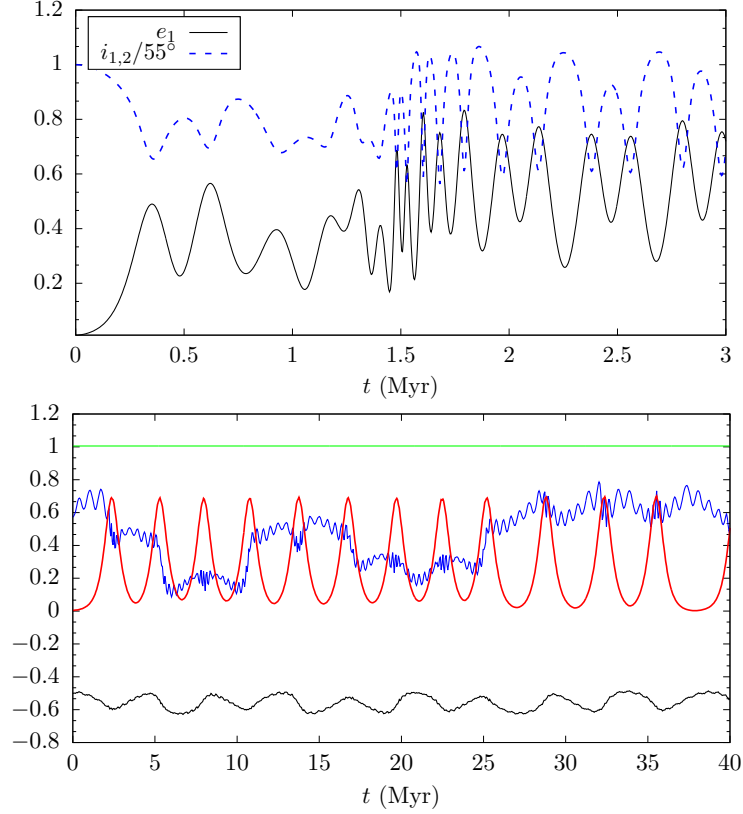


Figure 4.6: (Top) Kozai-like coupled oscillations of the e_1 and i_{12} in the 4-body system whose the initial parameters are given in Table 4.1. (Bottom) The blue curve represents the evolution of the projection of the angular momentum vector \mathbf{j}_1 along the direction of \mathbf{j}_2 , given by $j_{12} = \sqrt{1 - e_1^2} \cos(i_{12})$, and the black curve that of the outer planet along the direction of \mathbf{j}_3 , given by $j_{23} = \sqrt{1 - e_2^2} \cos(i_2)$. The red curve indicates the orbital eccentricity of the outer planet, e_2 . The constant green line gives the ratio of the angular momenta of the companion star to the total system, which implies that its orbital plane can be taken to be the fixed reference plane.

After $t = 1$ Myr, the effect of the companion star on the outer planet starts to manifest itself: the orbital eccentricity e_2 reaches its highest value ~ 0.7 , and this causes a dramatic increase in the amplitude of oscillation of j_{12} . Then, j_{12} continues to oscillate around a different value with a small amplitude. As the

system evolves, this process repeats: the effect of the companion star on the outer planet affects the outer planet's gravitational torque on the inner planet. This in turn creates differences in the oscillation amplitudes of e_1 and i_{12} .

The effect of the inner planet on the outer one is much smaller than that of the companion star, and thus the oscillations of e_2 and i_2 due to the companion star can be considered regular. Indeed, the amplitude and the period of the K-L cycles of e_2 and i_2 are constant. In Fig. 4.6 (bottom), we also display the ratio of the angular momenta of the companion star to the total system with the green line, which is constant and ~ 1 . The majority of the total angular momentum is carried by the companion star, and its orbital plane stays fixed in time. Therefore, under the perturbation from the stellar companion on a fixed orbit, the component of the angular momentum vector of the outer planet, \mathbf{j}_2 , along \mathbf{j}_3 oscillates about its initial value with a relatively smaller amplitude than j_{12} , which is illustrated with the black curve.

- Using the conservation of $j_{12} = \sqrt{1 - e_1^2} (\cos i_1 \cos i_2 + \sin i_1 \sin i_2 \cos \Delta\Omega)$ in Fig. 4.7, we draw the constant j_{12} curves which give us the evolution of the eccentricity and the inclination of the inner orbit. The initial values are $e_1 = 0.01$, $i_{12} = 55^\circ$ and $j_{12} = 0.57$. We can look at the $j_{12} = 0.57$ curve to examine the first 1 Myr of the evolution of the system. During that time, we may fix the angles $i_2 = 120^\circ$ and $\Delta\Omega = 0^\circ$ as if the outer planet's orbit were stationary. We see that i_1 oscillates between 65° and 170° , which is consistent with our simulations (Fig. 4.5).
- The sufficiently strong gravitational coupling among the planets allows them to stay stable as they secularly evolve despite their high mutual inclination, $i_{12} > 39^\circ$. The angular momentum vector \mathbf{j}_1 circulates around \mathbf{j}_2 while they rotate together around \mathbf{j}_3 . In this case, \mathbf{j}_1 undergoes nodal libration. As the inner planet can follow the nodal precession of the outer planet, i.e., the nodal offset $\Omega_1 - \Omega_2$ remains practically the same, the mutual inclination i_{12} oscillates about its initial value with a relatively smaller amplitude than that of i_1 .

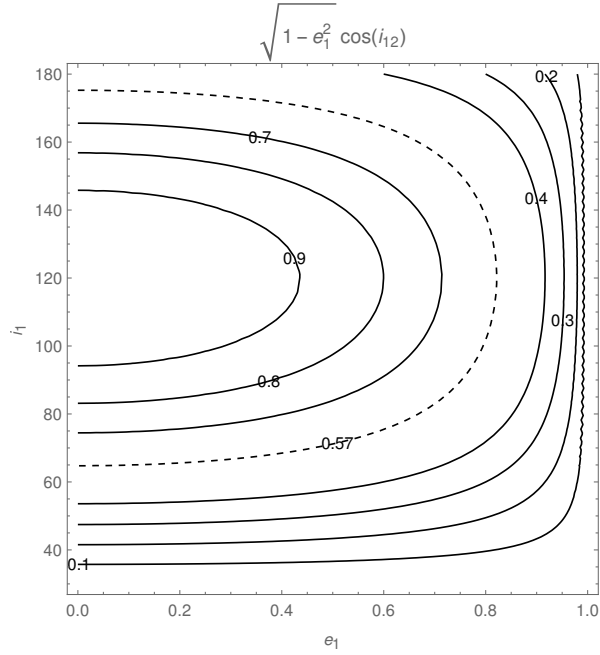


Figure 4.7: Different $j_{12} = \text{constant}$ curves representing the variations of eccentricity and inclination of the inner planet. Here, i_1 is measured from the orbital plane of the companion star, and initially $i_2 = 120^\circ$ and $\Delta\Omega = 0$. The dashed curve represents our system in Fig. 4.5, with $j_{12} = 0.57$.

- The dynamics of orbit flip differs in 3- and 4-body systems. In Fig. 3.3, the 3-body system consists of the inner and outer planets moving around the central star with the same initial setup in Table 4.1 except for $e_2 = 0.5$, $i_2 = 0^\circ$ and $m_3 = 0$. In this 3-body system, the orbit flip of the inner planet takes place with a time scale $t_{\text{oct}} \sim 10^7$ years via the EKL mechanism. In our 4-body system, we turn off the EKL mechanism by taking $e_2 \sim 0$, and set $i_2 = 120^\circ$. We see that i_1 grows monotonically to large values in a short time and crosses over 90° rapidly. By looking at Fig. 4.5, the timescale for the oscillation between the prograde and retrograde is $\sim 10^5$ years in the 4-body system, which is much smaller than in the 3-body case.

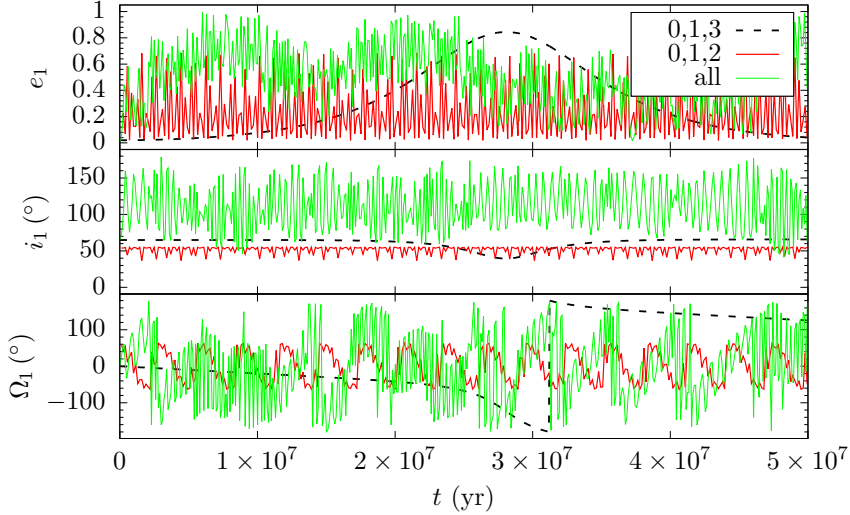


Figure 4.8: The evolution of the orbital parameters of the inner planet in two separate 3-body systems which are parts of the 4-body system in Table 4.1. The black dashed curve indicates the 3-body system consisting of the central star, the inner planet and the companion star, (0,1,3). Similarly, the solid red and green curves represent the 3-body system with (0,1,2) and the 4-body system with (0,1,2,3), respectively. Numerical simulations are carried out using the WHFast integrator with the integration time-step $dt = P_1/100$ years.

In Fig. 4.8, we examine the secular evolution of the orbital parameters of the inner planet in two separate 3-body systems consisting of the bodies (0,1,2) and (0,1,3) with the same initial parameters in Table 4.1. As expected, the inner planet’s orbital eccentricity and inclination undergo the standard K-L oscillations in the presence of perturbers (m_2 and m_3 separately) on circular orbits with different time scales. When we combine these systems, the total effect of the outer planet and the companion star on the inner planet enriches the dynamics of the system: e_1 is excited to large values and the orbit flip occurs, $65^\circ < i_1 < 170^\circ$.

4.3.1 Parameter space exploration

We try to find out which parts of the parameter space of 4-body systems may be able to induce orbit flips in circular orbits. The orbit flip in 4-body systems was studied in [22, 48]. Unlike their analyses, we investigate the flip conditions within the frame-

work of dynamical classification of 4-body systems, i.e., coupling of the planets. To this end, we present some of our numerical simulations that we obtain by changing the initial parameters of the system in Table 4.1. We fix the initial parameters of the inner planet and the companion star, and examine the rest of the parameter space to put constraints on the variables of the outer planet. We provide below some configurations of the system where the orbit of the inner planet always stays prograde and explain why orbit flip does not occur in those systems.

We start with turning off the planetary interactions by taking $m_2 = 0.03M_J$. The result of the simulation using the combination of the Gauss method and the TPO approximation is displayed in Fig. 4.9. The time scale of the K-L cycles of the inner planet due to the outer one is much larger than that due to the companion star: $t_{\text{KL},12} \gg t_{\text{KL},13}$. This time, the inner planet's eccentricity and inclination undergo the companion-star-driven K-L oscillations like the outer planet. In addition, the ratio of the time scale of the K-L cycles in (0,1,2) to that in (0,2,3) gets also very large $t_{\text{KL},12}/t_{\text{KL},23} \sim 200$. The evolution of the system is similar to the one in Fig. 4.1 : the angular momentum vectors \mathbf{j}_1 and \mathbf{j}_2 precess independently around the total angular momentum of the system, producing a high mutual inclination between the orbits of the planets. Unlike in Fig. 4.5, i_1 oscillates between 50° and 65° . As the planetary interactions are suppressed, the 4-body system behaves like two isolated 3-body systems consisting of (0,1,3) and (0,2,3). In this case, the cylindrical symmetry in these separate 3-body systems is conserved and orbit flip is not allowed.

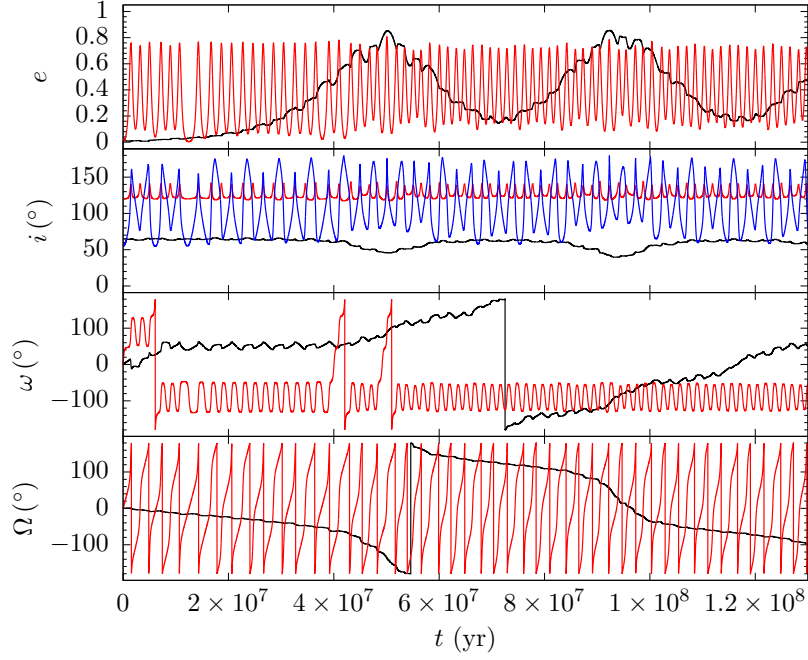


Figure 4.9: The evolution of a gravitationally decoupled two-planet system initially on circular and inclined orbits in the presence of a stellar companion. The initial orbital parameters of the system are the same as in Fig. 4.1, except for $m_2 = 0.03M_J$. The black (red) curves correspond to the inner (outer) planet. The blue curve represents the mutual inclination of the planets.

We also perform simulations where we take $i_2 = 60^\circ$. In Fig. 4.10, we see the rigid evolution of the planetary systems: their orbital planes precess at the same rate and thus the initial co-planarity $i_{12} = 5^\circ$ is maintained throughout their evolution. Also, the periods of the eccentricity-inclination oscillations are the same. This time, as i_{12} is less than the Kozai critical angle, the Kozai-like coupled oscillations of e_1 and i_{12} do not occur. Since the inner planet is strongly coupled to the outer one, i_1 cannot cross 90° while following i_2 , and thus it oscillates between $50^\circ < i_1 < 65^\circ$.

For the initial values of i_2 between 60° and 90° , the system cannot remain stable over time. In the K-L mechanism, we know that the amplitude of the eccentricity oscillation of e_2 increases with i_2 . When e_2 reaches very large values, the inner planet is ejected from the system, i.e. $e_1 > 1$. When $i_2 = 120^\circ$ as in Fig. 4.5, the outer planet's orbit is retrograde and effectively inclined by 60° relative to the orbital plane of the companion star, thus, the system can stay stable.

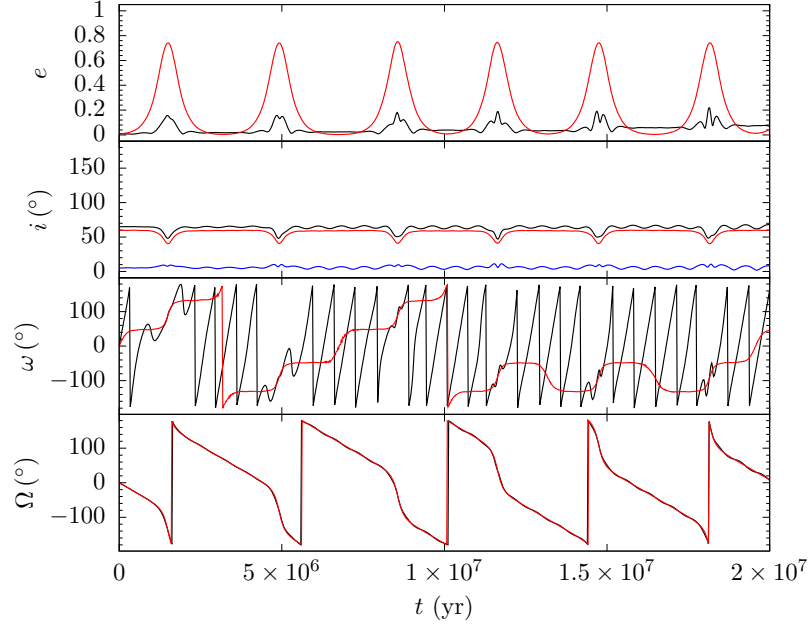


Figure 4.10: The evolution of a gravitationally coupled two-planet system initially on circular and coplanar orbits in the presence of a stellar companion. The initial orbital parameters of the system are the same as in Table 4.1 except for $i_2 = 60^\circ$. The black (red) curves correspond to the inner (outer) planet.

So far, we examined the decoupled-mutually-inclined and coupled-coplanar cases (Figs. 4.9 and 4.10, respectively) of two-planet systems in binaries separately and did not observe any orbit flip. We wonder what happens if we turn off the K-L oscillations of the outer planet due to the binary star by taking $i_2 = 5^\circ$ in Table 4.1. We present the simulation of this system in Fig. 4.11. This time, e_2 and i_2 oscillate with small amplitudes and thus the axial symmetry of the system is conserved. As a result, the inner orbit's inclination is restricted to be $i_1 < 90^\circ$.

These simulations indicate that the outer planet with a sufficiently inclined orbit can disturb the axial symmetry of the companion star. If the inner planet is affected by the torque of the outer one, its orbital orientation may flip.

Up to now, we investigated the possibility of the orbit flip in the presence of a fourth body, which is otherwise not possible. Now, we present the case where this time a fourth body prevents the orbit flip present in the existing system.

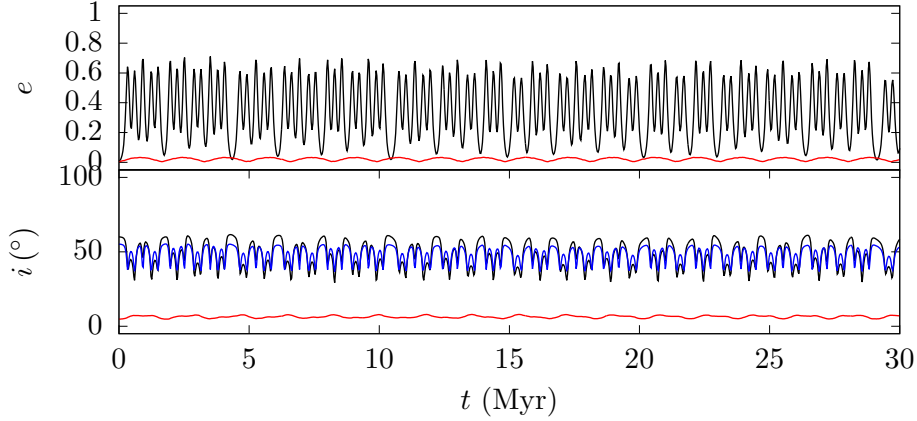


Figure 4.11: The evolution of a gravitationally coupled two-planet system initially on circular and inclined orbits in the presence of a stellar companion. The initial orbital parameters of the system are same as in Table 2.1 except $i_2 = 5^\circ$. The black (red) curves correspond to the inner (outer) planet.

We provide an example of this type of dynamical outcome in Fig. 4.13, where the presence of an additional body suppresses the effects of the EKL mechanism on the evolution of the 3-body system. At first, we consider a triple system consisting of two planets, where we set $i_{12} = 50^\circ$ and $e_2 = 0.5$. In Fig. 4.12, we see that octupole terms in the perturbing potential of the outer planet affect the evolution of the inner planet dramatically by flipping its orbit $i_{12} > 90^\circ$ and inducing large eccentricities e_1 .

Now, we add a companion star to the system. Fig. 4.13 demonstrates that the evolution of the inner planet's orbit is stabilized with respect to the EKL mechanism even if $e_2 = 0.5$. Under the gravitational torques from the companion star, the small contribution of octupole terms in the disturbing function of the outer planet cannot accumulate over many K-L cycles. As a result, the orbit flip of the inner planet does not occur, and the amplitude of the eccentricity e_1 oscillations becomes smaller. This effect is similar to the suppression of the K-L oscillations in 3-body systems with additional sources of periapsis precession.

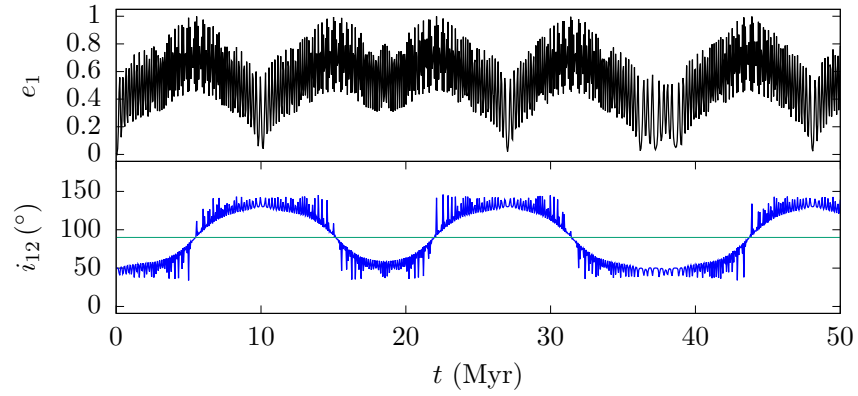


Figure 4.12: The evolution of the orbital eccentricity and inclination of the inner planet in the 3-body system as $m_3 \rightarrow 0$. The initial orbital parameters of the system are the same as in Table 4.1 except for $i_2 = 5^\circ$, $i_1 = 55^\circ$ and $e_2 = 0.5$. The orientation of the inner planet's orbit switches between prograde and retrograde (blue curves).

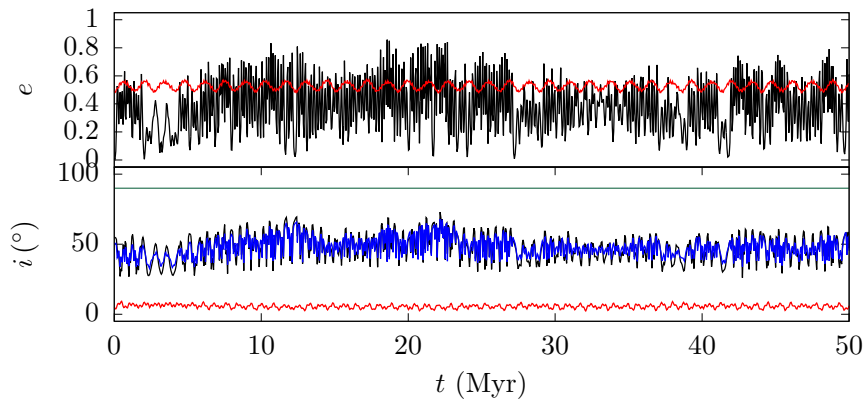


Figure 4.13: The evolution of the orbital eccentricity and inclination of the planets in the 4-body system whose initial orbital parameters are the same as in Table 4.1 except for $i_2 = 5^\circ$, $i_1 = 55^\circ$ and $e_2 = 0.5$. The black (red) curves correspond to the inner (outer) planet. The orbit flip of the inner planet is not observed here.

CHAPTER 5

DISCUSSION AND CONCLUSION

In this thesis, we investigated the secular evolution of two planets in a binary star system by decomposing it into three triples and combining two approximation methods. Each method possesses advantages over one another, yet suffers from certain limitations. The Gauss method is accurate to all orders in eccentricity and inclination but to the first order in mass. The TPO approximation is valid in the test particle limit and applicable for widely separated systems. Its upside is that the equations of motion have closed, though complicated, analytical forms. The implementation of the Gauss method is yet more difficult and time-consuming. With both methods, we numerically solved the averaged equations of motion and obtained the rate of change of the orbital elements in the long term. We tested the validity of these two secular approaches by comparing them with direct N -body simulations. All were in good agreement in terms of the period and the amplitude of the K-L oscillations.

We made the following approximations to simplify our analysis. As we were interested only in the secular evolution of systems, short-term dynamical effects such as mean-motion resonances and dissipative forces were neglected. With these simplifications, no energy exchange occurs between the bodies; instead they exchange angular momentum on the long time scales, namely of the order of million years. Consequently, the semi-major axes remain constant. In addition, we considered the bodies to be point masses, which eliminates tidal effects, and ignored all physical effects beyond the Newtonian gravity, e.g. general-relativistic precession.

Our numerical simulations show that the addition of a fourth body brings crucial effects to the dynamical evolution of 3-body systems. Depending on the initial setup of the system, it may cause significant changes in the orbital parameters of the ex-

isting system and even drive it to instability. The fourth body creates effects similar to that of the high-order (octupole) terms in the 3-body problem. For instance, the restrictions for the maximum eccentricity, $e_{\max} = [1 - (5/3) \cos^2 i_0]^{1/2}$, and the orientation, $i < 90^\circ$, are removed. On the other hand, the fourth body may suppress the slow but dramatic modulation of the Kozai-Lidov cycles due to octupole-order effects present in triple systems. This phenomenon is similar to the suppression of the EKL mechanism in 3-body systems with additional sources of periapsis precession such as general-relativistic precessions.

The strength of the gravitational coupling among the bodies determines the evolution and the stability of 4-body systems. In our work, we observe that especially weakly-coupled two-planet systems in binaries exhibit striking features and are more open to various dynamical outcomes, which includes the following:

- Despite the initially small inclinations ($i_1, i_2, i_{12} \ll 39^\circ$), the eccentricity of the inner planet can be excited to high values. The allowed region of the parameter space is limited: the orbital planes of the planets should not be nodally coupled so that the nodal precession of the outer one due to the companion star produces a nodal-offset $\Delta\Omega$, which in turn misaligns the initially coplanar orbits of the planets and thus starts the K-L mechanism for the inner one. As a result, the orbital eccentricity of the inner body becomes very large, provided that the induced K-L cycles are not suppressed by other dynamical effects.
- When $i_{12}, i_2 > 39^\circ$, the inner and outer planets are under the action of the K-L mechanism due to the outer planet and the companion star, respectively. If the K-L time scales for the subsystems (0,1,2) and (0,2,3) are comparable, $t_{\text{KL},12}/t_{\text{KL},23} \sim 1$, then extremely high orbital eccentricities and orbit flip can be observed for the inner planet. For this to happen, the time scale of the K-L mechanism acting on the inner planet due to the outer one must be smaller than that due to the companion star, i.e., $t_{\text{KL},12} < t_{\text{KL},13}$. Otherwise, the 4-body system will be made up of two isolated non-interacting 3-body systems.

APPENDIX A

SECULAR EQUATIONS OF MOTION

We provide the explicit expressions of the secular equations of motion in the test particle approximation. Since the ratio of the semi-major axes is much smaller than 1, $a'/a \ll 1$, and the mass of the perturbed particle is negligible, the majority of the angular momentum of the system is carried by the perturbing body. Therefore, the standard reference (XY) plane can taken to be the orbital xy plane of the perturbing body, which is assumed to be fixed. In this case, Ω is measured from the reference axis x . In addition, the angle i corresponds to the mutual inclination between the bodies. The angular momentum and the eccentricity vectors of the perturbed body, \mathbf{j}' and \mathbf{e}' respectively, can be written in the fixed coordinate system as

$$\begin{aligned} \mathbf{j}' &= j_x \hat{\mathbf{x}} + j_y \hat{\mathbf{y}} + j_z \hat{\mathbf{z}} \\ &= \sqrt{1 - e'^2} \begin{pmatrix} \sin i \sin \Omega \\ -\sin i \cos \Omega \\ \cos i \end{pmatrix}, \end{aligned} \tag{A.1}$$

$$\begin{aligned} \mathbf{e}' &= e_x \hat{\mathbf{x}} + e_y \hat{\mathbf{y}} + e_z \hat{\mathbf{z}} \\ &= e' \begin{pmatrix} \cos \omega \cos \Omega - \sin \omega \cos i \sin \Omega \\ \cos \omega \sin \Omega - \sin \omega \cos i \cos \Omega \\ \sin \omega \sin i \end{pmatrix} \end{aligned}$$

where $e' = (e_x^2 + e_y^2 + e_z^2)^{1/2}$ and $j' = (j_x^2 + j_y^2 + j_z^2)^{1/2}$.

We define $\tau = t/t_{\text{sec}}$, where $t_{\text{sec}} = \sqrt{\mathcal{G}M a'}/\Phi_0$. Then, the rates of change of these vectors in vectorial form are [28]

$$\begin{aligned} \frac{d\mathbf{j}'}{d\tau} &= -\mathbf{j}' \times \nabla_{\mathbf{j}'} \langle\langle \Phi \rangle\rangle - \mathbf{e}' \times \nabla_{\mathbf{e}'} \langle\langle \Phi \rangle\rangle, \\ \frac{d\mathbf{e}'}{d\tau} &= -\mathbf{j}' \times \nabla_{\mathbf{e}'} \langle\langle \Phi \rangle\rangle - \mathbf{e}' \times \nabla_{\mathbf{j}'} \langle\langle \Phi \rangle\rangle. \end{aligned} \tag{A.2}$$

Having derived the doubled-averaged interaction potential, we take its gradient in accordance with the operators

$$\begin{aligned}\nabla_{e'} &\equiv \frac{\partial}{\partial e_x} \hat{\mathbf{x}} + \frac{\partial}{\partial e_y} \hat{\mathbf{y}} + \frac{\partial}{\partial e_z} \hat{\mathbf{z}}, \\ \nabla_{j'} &\equiv \frac{\partial}{\partial j_x} \hat{\mathbf{x}} + \frac{\partial}{\partial j_y} \hat{\mathbf{y}} + \frac{\partial}{\partial j_z} \hat{\mathbf{z}}\end{aligned}\quad (\text{A.3})$$

and get

$$\begin{aligned}\nabla_{e'} \langle \langle \Phi \rangle \rangle &= \Phi_0 \left[\frac{3e_x}{2} + \frac{75}{64} \epsilon_{\text{Oct}} \left(\frac{1}{5} - \frac{16e_x^2}{5} + 7e_z^2 - \frac{8}{5} e^2 \right) - j_z^2 \right] \hat{\mathbf{x}} \\ &+ \Phi_0 \left[\frac{3e_y}{2} - \frac{15\epsilon_{\text{Oct}} e_x e_y}{4} \right] \hat{\mathbf{y}} \\ &+ \Phi_0 \left[-\frac{9e_z}{4} + \frac{75}{64} \epsilon_{\text{Oct}} \left(\frac{54e_x e_z}{5} - 2j_x j_z \right) \right] \hat{\mathbf{z}},\end{aligned}\quad (\text{A.4})$$

$$\nabla_{j'} \langle \langle \Phi \rangle \rangle = -\frac{75}{32} \Phi_0 \epsilon_{\text{Oct}} e_z j_z \hat{\mathbf{x}} + \Phi_0 \left[\frac{3j_z}{4} + \frac{75}{64} \epsilon_{\text{Oct}} (-2e_z j_x - 2e_x j_z) \right] \hat{\mathbf{z}}. \quad (\text{A.5})$$

Inserting Eqs. (A.5) and (A.6) into Eq. (A.3), we arrive at

$$\begin{aligned}\frac{d\mathbf{j}'}{d\tau} &= \frac{3}{32} [5(-8 + 35\epsilon_{\text{Oct}} e_x) e_y e_z - 25\epsilon_{\text{Oct}} e_y j_x j_z + 8j_y j_z \\ &- 25\epsilon_{\text{Oct}} j_y (e_z j_x + e_x j_z)] \hat{\mathbf{x}} + \frac{3}{64} [80e_x e_z - 16j_x j_z \\ &+ 5\epsilon_{\text{Oct}} (27e_z^3 + 20e_x j_x j_z + e_z(1 - 78e_x^2 - 8e_y^2 + 10j_x^2 \\ &- 15j_z^2))] \hat{\mathbf{y}} + \frac{15}{64} \epsilon_{\text{Oct}} [8e_y^3 + 10e_z j_y j_z + e_y(-1 + 8e_x^2 - 27e_z^2 + 5j_z^2)] \hat{\mathbf{z}}\end{aligned}\quad (\text{A.6})$$

and

$$\begin{aligned}\frac{d\mathbf{e}'}{d\tau} &= -\frac{3}{32} [8(3e_z j_y + e_y j_z) + 5\epsilon_{\text{Oct}} (5e_y e_z j_x - 27e_x e_z j_y \\ &- 3e_x e_y j_z + 5j_x j_y j_z)] \hat{\mathbf{x}} + \frac{3}{64} [4(12 - 55\epsilon_{\text{Oct}} e_x) e_z j_x + 16e_x j_z + 85\epsilon_{\text{Oct}} e_z^2 j_z \\ &- 5\epsilon_{\text{Oct}} j_z (-1 + 14e_x^2 + 8e_y^2 - 10j_x^2 + 5j_z^2)] \hat{\mathbf{y}} + \frac{3}{64} [(32 - 80\epsilon_{\text{Oct}} e_x) e_y j_x \\ &- 32e_x j_y + 40\epsilon_{\text{Oct}} e_y^2 j_y + 50\epsilon_{\text{Oct}} e_y e_z j_z + 5\epsilon_{\text{Oct}} j_y (-1 + 24e_x^2 - 27e_z^2 + 5j_z^2)] \hat{\mathbf{z}}.\end{aligned}\quad (\text{A.7})$$

Now, we can find the rate of change of the orbital elements using Eq. (2.21). In Eqs. (A.7) and (A-8), we write the Cartesian components of the vectors \mathbf{j}' and \mathbf{e}' in terms of the orbital parameters using Eqs. (A.1) and (A.2). Then, we combine these expressions into Eq.(2.21) and obtain the secular equations of motion in the TPO

approximation as [23]

$$\begin{aligned}
\frac{de'}{d\tau} &= \frac{d\mathbf{e}'}{d\tau} \cdot \hat{\mathbf{x}}' \\
&= \frac{15}{8} \sqrt{1-e'^2} \sin^2 i \sin 2\omega - \frac{15\sqrt{1-e'^2}\epsilon_{\text{oct}}}{512} \left\{ \cos \Omega \left[(4+3e'^2)(3+5\cos 2i) \right. \right. \\
&\quad \times \sin \omega + 210e'^2 \sin^2 i \sin 3\omega \left. \right] + 2 \cos i \cos \omega \sin \Omega \left[15(2+5e'^2) \cos 2i \right. \\
&\quad \left. \left. + 7(30e'^2 \cos 2\omega \sin^2 i - 2 - 9e'^2) \right] \right\}, \tag{A.8}
\end{aligned}$$

$$\begin{aligned}
\frac{di}{d\tau} &= \frac{-\sin \omega \hat{\mathbf{x}}' - \cos \omega \hat{\mathbf{y}}'}{j'} \cdot \frac{d\mathbf{j}'}{d\tau} \\
&= -\frac{15e'^2 \sin 2i \sin 2\omega}{16 \sqrt{1-e'^2}} + \frac{15\epsilon_{\text{oct}}e'}{256\sqrt{1-e'^2}} \left\{ 10 \sin 2i \cos 2\Omega \sin 2\omega (2+5e'^2 \right. \\
&\quad \left. + 7e'^2 \cos 2\omega) - \cos \omega \sin i \sin \Omega [26+37e'^2-35e'^2 \cos 2\omega] \right. \\
&\quad \left. - 15 \cos 2i (7e'^2 \cos 2\omega - 2 - 5e'^2) \right\}, \tag{A.9}
\end{aligned}$$

$$\begin{aligned}
\frac{d\Omega}{d\tau} &= \frac{\cos \omega \hat{\mathbf{x}}' - \sin \omega \hat{\mathbf{y}}'}{j' \sin i} \cdot \frac{d\mathbf{j}'}{d\tau} \\
&= \frac{3 \cos i (5e'^2 \cos^2 \omega - 4e'^2 - 1)}{4 \sqrt{1-e'^2}} + \frac{15e'\epsilon_{\text{oct}}}{128\sqrt{1-e'^2}} \left\{ 20 \cos i \cos \omega \cos \Omega \right. \\
&\quad \times (2+5e'^2-7e'^2 \cos 2\omega) + \left[35e'^2(1+3\cos 2i) \cos 2\omega - 46 - 17e'^2 \right. \\
&\quad \left. \left. - 15(6+e'^2) \cos 2i \right] \sin \omega \sin \Omega \right\}, \tag{A.10}
\end{aligned}$$

$$\begin{aligned}
\frac{d\omega}{d\tau} &= \frac{\mathbf{e}' \cdot \hat{\mathbf{x}}'}{e'} - \dot{\Omega} \cos i \\
&= \frac{32(1-e'^2) + 5 \sin \omega^2 (e'^2 - \sin^2 i)}{4 \sqrt{1-e'^2}} + \frac{15\epsilon_{\text{oct}}}{64} \left\{ \frac{e' \cos i}{\sqrt{1-e'^2}} \left[\sin \omega \sin \Omega \right. \right. \\
&\quad \times [10(3\cos^2 i - 1)(1-e'^2) + A] - 5B \cos i \cos \Theta \left. \right] - \frac{\sqrt{1-e'^2}}{e'} \\
&\quad \left. \times \left[10 \sin \omega \sin \Omega \cos i \sin^2 i (1-3e'^2) + \cos \Theta (3A - 10 \cos^2 i + 2) \right] \right\} \tag{A.11}
\end{aligned}$$

where

$$\begin{aligned} A &\equiv 4 + 3e'^2 - \frac{5}{2}B \sin i^2, \\ B &\equiv 2 + 5e'^2 - 7e'^2 \cos 2\omega, \\ \cos \Theta &\equiv \cos \omega \cos \Omega - \cos i \sin \omega \sin \Omega. \end{aligned} \tag{A.12}$$

APPENDIX B

CALCULATION OF THE ELLIPTIC INTEGRALS

In the numerical calculations, we evaluate the elliptic integrals using the Chebyshev series expansions. The power series expansion of a function $f(x)$, defined on the interval $0 \leq x \leq 1$, using the shifted Chebyshev polynomials is given by

$$f(x) = \sum'_{n=0}^{\infty} a_n T_n^*(x), \quad (\text{B.1})$$

where

$$T_n^*(x) = \cos[n \arccos(2x - 1)]. \quad (\text{B.2})$$

Here the primed summation, \sum' , implies that $n = 0$ term is to be multiplied by $1/2$. The expressions for the expansion of the complete elliptic integral of the first and second kind are [53]

$$K(k) = \pi \sum'_{n=0}^{\infty} b_n T_n^*(2k^2), \quad (\text{B.3})$$

$$E(k) = \sum'_{n=0}^{\infty} p_n T_n^*(2k^2) \quad (\text{B.4})$$

where $0 \leq k^2 \leq \frac{1}{2}$. We present the coefficients b_n and p_n in Table B.1 and B.2 [53]. This method, with such few terms, provides much more rapid numerical evaluation than traditional computational packages.

Table B.1: The Chebyshev coefficients for the expansion of the complete elliptic integral of the first kind, $K(k)$.

n	b_n				
0	1.08154	45545	59937	18609	6290
1	.04457	32214	32776	36906	7285
2	.00424	57603	69819	50477	5625
3	.00050	26127	97966	24604	6695
4	.00006	57701	68092	91332	4847
5		91171	11066	72370	1032
6		13120	28529	09857	8893
7		1938	36613	34712	5696
8		291	99279	32665	4288
9		44	64889	07318	4542
10		6	90892	11906	9053
11		1	07945	77920	1563
12			17001	18928	9808
13			2695	77141	0000
14			429	92125	4075
15			68	90586	9287
16			11	09198	9146
17			1	79234	8951
18				29060	8238
19				4726	1548
20				770	7066
21				125	9903
22				20	6421
23				3	3889
24					5574
25					918
26					152
27					25
28					4
29					1

Table B.2: The Chebyshev coefficients for the expansion of the complete elliptic integral of the second kind, $E(k)$.

n		p_n				
0		2.92822	58504	05146	88299	9545
1	-	.10983	85572	43451	91176	2083
2	-	.00337	07796	33972	36148	2362
3	-	.00023	53008	58731	36941	4039
4	-	.00002	17641	44792	00668	4306
5	-		23301	64928	43946	8235
6	-		2729	92738	83921	9275
7	-		339	98892	03979	0023
8	-		44	25755	44400	3036
9	-		5	95739	31848	8316
10	-			82323	46149	6100
11	-			11618	87697	1255
12	-			1668	57756	6166
13	-			243	13006	2812
14	-			35	86643	5645
15	-			5	34740	3815
16	-				80463	4863
17	-				12205	7159
18	-				1864	7874
19	-				286	7194
20	-				44	3363
21	-				6	8912
22	-				1	0761
23	-					1687
24	-					266
25	-					42
26	-					7
27	-					1

APPENDIX C

PYTHON CODES

Our Python codes for the numerical simulations of the 4-body systems considered in this thesis have been uploaded to the GitHub repository `MS_THESIS_4-body` by the username `fulyak`¹. This repository contains the following codes:

- (1) The REBOUND code: This code simulates a generic 4-body system by using REBOUND package. The number of bodies can be increased as desired. The simulation employs the WHFast integrator. The numerical analysis deals with exact Newton's equations of motion in the Jacobi coordinates. To minimize the error in the energy, one has to choose a time scale smaller than the orbital period of the bodies. As an output, one can obtain the position, velocity, orbital parameters, total energy and angular momentum, etc. of the bodies.
- (2) The REBOUND code with loop: In addition to the previous code, this one can loop over the orbital elements, masses and time parameters to scan various parts of the parameter space. The initial data should be provided externally by creating a type of batch file named `input`. The results are appended to one another for each loop in a single output file.
- (3) The Gauss-TPO code: We prepared this code to simulate the secular evolution of 4-body systems for this thesis. The system of our interest is made up of a central star, two planets and a companion star. In this code, we use the combination of the Gaussian ring algorithm and the test particle octupole approximation. For the interaction between the two planets, which can be closely separated, we use the Gaussian ring algorithm with a softening parameter b . For the effect of the companion star, we use the Hamiltonian perturbation theory, where the ratio of

¹ See https://github.com/fulyak/MS_THESIS_4-body/

the semi-major axes is expanded up to octupole order in the disturbing function of the companion star. Additionally, since the mass of each planet is much smaller than that of the companion star, the test particle approximation is used, i.e., the planets do not affect the companion star and its orbital plane is approximated to be fixed. The double averaged equations of motion are integrated using the Bulirsch-Stoer (BS) integrator with much larger time scales than the orbital periods. In the Gaussian ring algorithm, first a single average is performed over the orbit of a perturbing body analytically. Then, another average is taken over the orbit of the perturbed body using the discrete Fourier transform. In this numerical analysis, the orbit of the perturbed body is divided into N equally spaced points in eccentric anomaly. One has to choose a suitable value of N to minimize the energy error. Also, the BS integrator introduces its own tolerance. As an output, one can obtain the orbital parameters and angular momenta of the bodies.

REFERENCES

- [1] M. Holman, J. Touma, and T. S., “Chaotic variations in the eccentricity of the planet orbiting 16 Cygni B,” *Nature*, vol. 386, pp. 254–256, 1997.
- [2] K. A. Innanen, J. Q. Zheng, S. Mikkola, and M. J. Valtonen, “The Kozai Mechanism and the Stability of Planetary Orbits in Binary Star Systems,” *The Astrophysical Journal*, vol. 113, p. 1915, 1997.
- [3] T. Mazeh, Y. Krymolowski, and G. Rosenfeld, “The High Eccentricity of the Planet Orbiting 16 Cygni B,” *The Astrophysical Journal*, vol. 477, no. 2, pp. L103–L106, 1997.
- [4] M. L. Lidov, “The evolution of orbits of artificial satellites of planets under the action of gravitational perturbations of external bodies,” *Planetary and Space Science*, vol. 9, pp. 719–759, 1962.
- [5] Y. Kozai, “Secular perturbations of asteroids with high inclination and eccentricity,” *The Astrophysical Journal*, vol. 67, p. 591, 1962.
- [6] R. S. Harrington, “Dynamical evolution of triple stars,” *The Astrophysical Journal*, vol. 73, pp. 190–194, 1968.
- [7] A. Morbidelli, *Modern celestial mechanics : aspects of solar system dynamics*. London, New York, Taylor & Francis, 2002.
- [8] I. I. Shevchenko, ed., *The Lidov-Kozai Effect - Applications in Exoplanet Research and Dynamical Astronomy*, vol. 441 of *Astrophysics and Space Science Library*. 2017.
- [9] E. B. Ford, B. Kozinsky, and F. A. Rasio, “Secular Evolution of Hierarchical Triple Star Systems,” *The Astrophysical Journal*, vol. 605, no. 2, pp. 966–966, 2004.
- [10] R. A. Broucke, “Long-Term Third-Body Effects via Double Averaging,” *Journal of Guidance, Control, and Dynamics*, vol. 26, no. 1, pp. 27–32, 2003.

- [11] R. Malhotra, “Orbital resonances in planetary systems,” *Encyclopedia of Life Support Systems by UNESCO*, vol. 6.119.55, p. 31, 2012.
- [12] M. L. Lidov and S. L. Ziglin, “Non-restricted double-averaged three body problem in Hill’s case,” *Celestial mechanics*, vol. 13, no. 4, pp. 471–489, 1976.
- [13] P. P. Eggleton and L. Kisseleva-Eggleton, “A mechanism for producing short-period binaries,” *Astrophysics and Space Science*, vol. 304, no. 1, pp. 75–79, 2006.
- [14] D. Fabrycky and S. Tremaine, “Shrinking Binary and Planetary Orbits by Kozai Cycles with Tidal Friction,” *The Astronomical Journal*, vol. 669, pp. 1298–1315, 2007.
- [15] Y. Lithwick and S. Naoz, “The Eccentric Kozai Mechanics for a Test Particle,” *The Astrophysical Journal*, vol. 742, no. 2, p. 94, 2011.
- [16] S. Naoz, W. M. Farr, and F. A. Rasio, “On the Formation of Hot Jupiters in Stellar Binaries,” *The Astrophysical Journal*, vol. 754, no. 2, p. L36, 2012.
- [17] B. Katz, S. Dong, and R. Malhotra, “Long-Term Cycling of Kozai-Lidov Cycles: Extreme Eccentricities and Inclinations Excited by a Distant Eccentric Perturber,” *Phys. Rev. Lett.*, vol. 107, p. 181101, 2011.
- [18] S. Naoz, W. M. Farr, Y. Lithwick, F. A. Rasio, and J. Teyssandier, “Secular dynamics in hierarchical three-body systems,” *Monthly Notices of the Royal Astronomical Society*, vol. 431, no. 3, pp. 2155–2171, 2013.
- [19] G. Li, S. Naoz, B. Kocsis, and A. Loeb, “Eccentricity Growth and Orbit Flip in Near-coplanar Hierarchical Three-body Systems,” *The Astrophysical Journal*, vol. 785, p. 116, 2014.
- [20] J. Teyssandier, S. Naoz, I. Lizarraga, and F. A. Rasio, “Extreme Orbital Evolution from Hierarchical Secular Coupling of Two Giant Planets,” *The Astrophysical Journal*, vol. 779, no. 2, p. 166, 2013.
- [21] R. A. Mardling and D. N. C. Lin, “Calculating the Tidal, Spin, and Dynamical Evolution of Extrasolar Planetary Systems,” *The Astrophysical Journal*, vol. 573, no. 2, pp. 829–844, 2002.

- [22] A. S. Hamers, H. B. Perets, F. Antonini, and S. F. Portegies Zwart, “Secular dynamics of hierarchical quadruple systems: the case of a triple system orbited by a fourth body,” *Monthly Notices of the Royal Astronomical Society*, vol. 449, no. 4, pp. 4221–4245, 2015.
- [23] B. Pu and D. Lai, “Eccentricities and inclinations of multiplanet systems with external perturbers,” *Monthly Notices of the Royal Astronomical Society*, vol. 478, no. 1, pp. 197–217, 2018.
- [24] G. Takeda, R. Kita, and F. A. Rasio, “Planetary Systems in Binaries. I. Dynamical Classification,” *The Astrophysical Journal*, vol. 683, no. 2, pp. 1063–1075, 2008.
- [25] J. R. Touma, S. Tremaine, and M. V. Kazandjian, “Gauss’s method for secular dynamics, softened,” *Monthly Notices of the Royal Astronomical Society*, vol. 394, no. 2, pp. 1085–1108, 2009.
- [26] C. Murray and S. Dermott, *Solar System Dynamics*. Cambridge, UK: Cambridge University Press, 2000.
- [27] J. Morehead, “Visualizing the extra symmetry of the Kepler problem,” *American Journal of Physics*, vol. 73, no. 3, pp. 234–239, 2005.
- [28] S. Tremaine and T. D. Yavetz, “Why do Earth satellites stay up?,” *American Journal of Physics*, vol. 82, no. 8, pp. 769–777, 2014.
- [29] A. J. Rosengren and D. J. Scheeres, “On the Milankovitch orbital elements for perturbed Keplerian motion,” *Celestial Mechanics and Dynamical Astronomy*, vol. 118, pp. 197–220, 2014.
- [30] P. P. Eggleton, L. G. Kiseleva, and P. Hut, “The Equilibrium Tide Model for Tidal Friction,” *The Astrophysical Journal*, vol. 499, no. 2, pp. 853–870, 1998.
- [31] C. Gauss, “Omnem Functionem Algebraicam Rationalem Integram,” <http://resolver.sub.uni-goettingen.de/purl?PPN235999628> (in Latin), vol. 331, 1866.
- [32] G. W. Hill, “Secular Perturbations of the Planets,” *American Journal of Mathematics*, vol. 23, no. 4, pp. 317–336, 1901.

- [33] B. Gladman, “Dynamics of systems of two close planets,” *Icarus*, vol. 106, p. 247, 1993.
- [34] S. Doolin and K. M. Blundell, “The dynamics and stability of circumbinary orbits,” *Monthly Notices of the Royal Astronomical Society*, vol. 418, no. 4, pp. 2656–2668, 2011.
- [35] P. Musen, “A discussion of Halphen’s method of secular perturbations and its application to the determination of long-range effects in the motion of celestial bodies,” *Reviews of Geophysics*, vol. 1, no. 1, 1963.
- [36] S. Naoz, “The Eccentric Kozai-Lidov Effect and Its Applications,” *Annual Review of Astronomy and Astrophysics*, vol. 54, no. 1, pp. 441–489, 2016.
- [37] S. Tremaine, J. Touma, and F. Namouni, “Satellite Dynamics on the Laplace Surface,” *The Astronomical Journal*, vol. 137, no. 3, pp. 3706–3717, 2009.
- [38] C. Petrovich, “Steady-State Planet Migration by the Kozai-Lidov Mechanism in Stellar Binaries,” *The Astrophysical Journal*, vol. 799, no. 1, p. 27, 2015.
- [39] R. Bulirsch and J. Stoer, “Numerical treatment of ordinary differential equations by extrapolation methods,” *Numerische Mathematik*, vol. 8, no. 1, pp. 1–13, 1966.
- [40] H. Rein and D. Tamayo, “whfast: a fast and unbiased implementation of a symplectic Wisdom–Holman integrator for long-term gravitational simulations,” *Monthly Notices of the Royal Astronomical Society*, vol. 452, no. 1, pp. 376–388, 2015.
- [41] J. Wisdom and M. Holman, “Symplectic maps for the N-body problem.,” *The Astrophysical Journal*, vol. 102, pp. 1528–1538, 1991.
- [42] B. Liu, D. J. Muñoz, and D. Lai, “Suppression of extreme orbital evolution in triple systems with short-range forces,” *Monthly Notices of the Royal Astronomical Society*, vol. 447, no. 1, pp. 747–764, 2014.
- [43] R. A. Wittenmyer, M. Endl, and W. D. Cochran, “Long-Period Objects in the Extrasolar Planetary Systems 47 Ursae Majoris and 14 Herculis,” *The Astrophysical Journal*, vol. 654, no. 1, pp. 625–632, 2007.

- [44] H. Sana, S. E. de Mink, A. de Koter, N. Langer, C. J. Evans, M. Gieles, E. Gosset, R. G. Izzard, J.-B. Le Bouquin, and F. R. N. Schneider, “Binary Interaction Dominates the Evolution of Massive Stars,” *Science*, vol. 337, no. 6093, pp. 444–446, 2012.
- [45] D. E. Trilling, J. A. Stansberry, K. R. Stapelfeldt, G. H. Rieke, K. Y. L. Su, R. O. Gray, C. J. Corbally, G. Bryden, C. H. Chen, A. Boden, and C. A. Beichman, “Debris Disks in Main-Sequence Binary Systems,” *The Astrophysical Journal*, vol. 658, no. 2, pp. 1289–1311, 2007.
- [46] L. A. Saleh and F. A. Rasio, “The Stability and dynamics o planets in tight binary systems,” *The Astrophysical Journal*, vol. 694, no. 2, pp. 1566–1576, 2009.
- [47] G. Takeda, R. Kita, F. A. Rasio, and S. M. Rubinstein, “Secular Evolution of Planetary Systems in Binaries,” *Astronomical Society of the Pacific Conference Series*, vol. 398, p. 209, 2008.
- [48] O. Pejcha, J. M. Antognini, B. J. Shappee, and T. A. Thompson, “Greatly enhanced eccentricity oscillations in quadruple systems composed of two binaries: implications for stars, planets and transients,” *Monthly Notices of the Royal Astronomical Society*, vol. 435, pp. 943–951, 2013.
- [49] R. Schwarz, B. Funk, R. Zechner, and A. Bazsó, “New prospects for observing and cataloguing exoplanets in well-detached binaries,” *Monthly Notices of the Royal Astronomical Society*, vol. 460, no. 4, pp. 3598–3609, 2016.
- [50] S. R. Kane *et al.*, “Evidence for Reflected Light from the Most Eccentric Exoplanet Known,” *The Astrophysical Journal*, vol. 821, no. 1, p. 65, 2016.
- [51] J. T. Wright *et al.*, “The Exoplanet Orbit Database,” *Publications of the Astronomical Society of the Pacific*, vol. 123, no. 902, pp. 412–422, 2011.
- [52] A. Hale, “Orbital coplanarity in solar-type binary systems: Implications for planetary system formation and detection,” *The Astrophysical Journal*, vol. 107, pp. 306–332, 1994.
- [53] W. J. Cody, “Chebyshev polynomial expansions of complete elliptic integrals,” *Mathematics of Computation*, vol. 19, pp. 249–259, 1965.